Fall 2006

Flow characteristics and phase interactions of evaporating sprays in gas-solid suspensions

Muhammad Mushahid Rafique Qureshi
New Jersey Institute of Technology

ABSTRACT

FLOW CHARACTERISTICS AND PHASE INTERACTIONS OF EVAPORATING SPRAYS IN GAS-SOLID SUSPENSIONS

by

Muhammad Mushahid Rafique Qureshi

Evaporating spray jets have a wide range of applications in many industrial processes such as fluidized catalytic cracking of crude oil in petroleum refinery, coal gasification, fluidized coking to make synthetic crude oil, and condensed mode gas polymerization. The rapid evaporation of spray jets significantly affects the gas-solids mixing, solids concentration, gas/solids temperature and gas/solids velocity acceleration. The complex interactions mechanism of phase change, three phase interaction, heat and mass transfer of gas, solids and evaporating droplets dominate the process efficiency and product quality. In such three-phase flows, the phase transport characteristics are influenced by both droplet-gas interaction and droplet-solid interactions. In dense phase flow, the droplet-solid interaction becomes to play a dominant role in the transport of both spray and gas-solid flow. In very hot environments of gas-solid suspensions, the rapid vaporization of sprays results from the droplet-solids collisions. With the preheated temperature of solids beyond the Leidenfrost temperature, the heat transfer into spray droplets and resulted vaporization can be greatly restricted by the film boiling characteristics that are in turn coupled with collision dynamics. So far few studies on these complex yet important interaction mechanisms have been reported.

This doctoral dissertation study is aimed to gain an in-depth understanding on characteristic interactions among spray, gas and solids. The study is focused on cases where the rapid vaporization concurs with the spray injection into a gas-solid suspension

that is preheated beyond the Leidenfrost temperature. A combined study of experiments, mechanistic modeling and numerical simulations is thus conducted to investigate three fundamental effects or mechanisms: (1) effect of vaporization on gas entrainment in a submerge spray jet; (2) jet characteristics of sprays from rectangular nozzles with a fan angle; and (3) dynamic transport in a type-II Leidenfrost collision (between a small hot solid particle and a large droplet).

In the gas entrainment study, a direct measurement method is developed to study the air entrainment induced by a liquid nitrogen spray jet into an unbounded and stagnant room air. The air entrainment is determined by measurements of local oxygen concentration using an *in-situ* oxygen concentration analyzer, gas temperature using a thermocouple system, and droplet velocity using a Laser Doppler Velocimeter. The results not only support the approximation of flow similarities in evaporating sprays with round nozzles but also suggest that the evaporation of spray markedly weakens the gas entrainment. In addition, a parametric model is developed to provide a theoretical basis of the data analysis for the cross-section averaged spray evaporation rate within the spray jet region.

A three-dimensional simulation study is performed to investigate the hydrodynamic behaviors of a cross-flow liquid nitrogen spray injected into an air-FCC riser of rectangular cross-section. The gas-solid (air-FCC) flow is simulated using the multi-fluid method while the evaporating sprays (liquid nitrogen) are calculated using the Lagrangian trajectory method, with a strong two-way coupling between the two. Two parametric effects are studied in details here: (1) effect of aspect ratio of rectangular nozzles on flow characteristics and (2) effect of nozzle fan angle on spray coverage as

well as vapor flux distribution. The study concludes that there exists an optimized value of aspect ratio for which the spray coverage area is maximized. The simulation also shows the formation of a dense layer of solids around the spray from the compression effect of vapor expansion and rigid wall of gas-solids flow chamber. It is also found that the spray coverage is basically dominated by the spray fan angle. The spray vaporization flux per unit area of spray coverage is highly non-linearly distributed along the spray penetration.

Interaction mechanism of large spray droplets and small solid particles is the key factor to govern the phase interactions of the spray in gas-solid flows as most of the evaporation of spray occurs in the initial part of spray jet as concluded by the fist two parts of this thesis. A careful analysis of this system reveals that this interaction mechanism is basically different than that of Leidenfrost collision between a small droplet and a large solid particle (defined as Type I Leidenfrost collision here). Portion of this study is thus focused on the heat and mass transfer during the Leidenfrost collisions between large evaporating droplets and small solid particles (defined as Type II Leidenfrost collision). In this study, experiments are conducted first to identify various modes of Type II Leidenfrost collision, and then basic mechanistic models have been developed to describe these modes. Parametric effects of different particle temperatures and velocities on the heat and mass transfer during the collision process have been illustrated using these models.

FLOW CHARACTERISTICS AND PHASE INTERACTIONS OF EVAPORATING SPRAYS IN GAS-SOLID SUSPENSIONS

by
Muhammad Mushahid Rafique Qureshi

A Dissertation
Submitted to the Faculty of
New Jersey Institute of Technology
in Partial Fulfillment of the Requirements for the Degree of
Doctor of Philosophy in Mechanical Engineering

Department of Mechanical Engineering

January 2007

APPROVAL PAGE

FLOW CHARACTERISTICS AND PHASE INTERACTIONS OF EVAPORATING SPRAYS IN GAS-SOLID SUSPENSIONS

Muhammad Mushahid Rafique Qureshi

Dr. Chao Zhu, Dissertation Advisor — Date
Associate Professor of Mechanical Engineering, NJIT

Dr. Pushpendra Singh, Committee Member — Date
Professor of Mechanical Engineering, NJIT

Dr. Edward L. Dreizin, Committee Member — Date
Professor of Mechanical Engineering, NJIT

Dr. Ernest Geskin, Committee Member — Date
Professor of Mechanical Engineering, NJIT

Dr. Teh C. Ho, Committee Member — Date
Sr. Research Associates, Corporate Strategic Research Laboratories
ExxonMobil Research and Engineering Co., Annandale, NJ

BIOGRAPHICAL SKETCH

Author: Muhammad Mushahid Rafique Qureshi

Degree: Doctor of Philosophy

Date: January 2007

Undergraduate and Graduate Education:

- Doctor of Philosophy in Mechanical Engineering,
  New Jersey Institute of Technology, Newark, NJ, 2007

- Master of Science in Mechanical Engineering,
  New Jersey Institute of Technology, Newark, NJ, 2003

- Bachelor of Science in Mechanical Engineering,
  University of Engineering and Technology, Lahore, Pakistan, 2000

Major: Mechanical Engineering

Presentations and Publications:

Muhammad Mushahid Rafique Qureshi and Chao Zhu,
"Gas Entrainment in an Evaporating Spray jet,"
International Journal of Heat and Mass Transfer 49 (2006) 3417-3428.

Muhammad Mushahid Rafique Qureshi, and Chao Zhu,
"Crossflow Evaporating Sprays in Gas-Solid Flows: Effect of Aspect Ratio of Rectangular Nozzles,"
Powder Technology 166 (2006) 60-71.

Muhammad M. R. Qureshi, Chao Zhu, Chao-Hsin Lin, Liang-Shih Fan,
"Effect of Nozzle Fan Angle on Sprays in Gas-Solid Riser Flow,"
China Particuology 4(3-4) (2006) 147-152.

Tong Lee, Muhammad M. Rafique Qureshi, Xiaohua Wang, Chao Zhu,
"3-D Simulations of Crossflow Evaporating Spray in Circulating Fluidized Beds,"
To be submitted to AIChE Journal.

Guangliang Liu, Muhammad M. Rafique Qureshi, Edward L. Dreizin, Chao Zhu,
"Droplet-Particle Collision over Leidenfrost Temperature"
To be submitted to International Journal of Heat and Mass Transfer.

Muhammad Mushahid Rafique Qureshi and Chao Zhu,
"Crossflow Evaporating Sprays in Gas-Solid Flows: Effect of Aspect Ratio of Rectangular Nozzles"
Frontiers in Applied and Computational Mathematics, May 15-16 (2006) Newark, NJ, USA.

Rafique Qureshi, Muhammad M., Lee T., Yu Q., Zhu C.,
"Measurements of Gas Entrainment in Evaporating Spray Jets,"
Proceedings of HTFED04 2004 ASME Heat Transfer/Fluids Engineering Summer Conference, July 11–15 (2004) Charlotte, NC, USA.

Rafique Qureshi, Muhammad M., Lee T., Yu Q., Zhu C.,
"Crossflow Evaporating Spray: Effect of Aspect Ratio of Rectangular Nozzles"
AIChE Annual Meeting, November 16-21 (2003) San Francisco, CA, USA.

To my beloved parents, my wife, and family

ACKNOWLEDGMENT

I would like to thank Almighty Allah (SWT) for His countless blessings throughout my life. I would like to express my deepest appreciation to Dr. Chao Zhu, who not only served as my research supervisor, providing valuable and countless resources, insight, and intuition, but also constantly gave me support, encouragement, and reassurance. I would also like to acknowledge Dr. Edward L. Dreizin in providing a much needed experimental support for a portion of this study. Special thanks are given to Dr. Pushpendra Singh, Dr. Ernest Geskin and Dr. Teh C. Ho for actively participating in my committee.

I would like to thank Dr. Marty Kashef of Chilworth Technology Inc. for providing me with an opportunity in his company and his support in easing my schedule towards the end of my studies.

Many of my fellow graduate students; Dr. Qun Yu, Dr. Tong Lee, Jun Yu and Dawei Wang in the Particulate Multiphaseflow Laboratory are deserving of recognition for their support. I also wish to thank ExxonMobil Research and Engineering Co. for providing financial resources for this project.

I would like to sincerely thank my beloved parents, my wife, my baby, and all other family members for their support and encouragement throughout my academic career.

TABLE OF CONTENTS

TABLE OF CONTENTS
(Continued)

TABLE OF CONTENTS
(Continued)

TABLE OF CONTENTS
(Continued)

Chapter **Page**

LIST OF TABLES

LIST OF FIGURES

LIST OF FIGURES
(Continued)

LIST OF FIGURES
(Continued)

Figure **Page**

CHAPTER 1

INTRODUCTION

1.1 Background

Evaporating spray jets are used in many industrial applications such as feed oil sprays in the petroleum refinery, spray drying, liquid fuel sprays in engine combustion, and spray-assisted coal gasification. Spray with a rapid evaporation can have a strong influence on flow characteristics such as spray penetration length, spray trajectory deflection and can strongly influence the phase interactions with the secondary medium. Nozzle characteristics, such as shape, dimensions, and fan angle have a significant effect on the spray characteristics and behavior especially in the presence of a strong interacting secondary medium. Hence, it is interesting to investigate the interacting effects to fully understand and govern the flow behavior. However, this problem is very challenging due to its very complicated phase interaction mechanism and also due to the complexity in measurement methods used in these studies. Therefore, almost all studies focus on the circular shape nozzle due to its symmetry around the axis which is useful for modeling purposes. Academically, this problem has been attempted many times and a reasonable understanding has been achieved. For a cross flow circular nozzle, studies are underway and some understanding has already been achieved. Interestingly, it has been experimentally found that rectangular configuration of nozzle provides much better results for above mentioned industrial applications and is of primary interest for the research point of view. It is very important to note that rectangular shape nozzles behave much differently than

circular nozzles in terms of flow characteristics. Axial similarities may and may not hold. Nozzle fan angle (spray spreading angle) and orientation of the rectangular nozzle (horizontal to vertical) add to the complexity of the problem. Moreover to investigate this problem in the presence of a highly evaporating medium makes it very challenging yet exciting.

1.2 Purpose of Study

Spray characteristics such as entrainment of the secondary medium into the spray, aspect ratio of the rectangular nozzle, effect of fan angle on the flow structure are all unanswered questions in this field of study. A detailed study is required to see the effect of these parameters on the flow structure. An experimental approach is adapted to quantify the parametric effects on the flow structure. However, as it is very hard to quantify every possible parameter experimentally, a numerical study is performed to investigate the effects of these parameters in detail.

Although a qualitative analysis is possible with the experimental investigations, it is very necessary to develop mechanistic models to interpret the experimental data to identify and then calculate the useful information to solve a complex phenomenon such as entrainment of surrounding medium by evaporating spray jets. This study focuses on the basic development of the methodology to quantify the entrainment characteristic of a two phase spray jet. The successful results of this study may form the development of advanced and more sophisticated methods which can be implemented into the real industrial applications.

It is also very important to realize the industrial application methods and provide first-hand approximate solutions for the basic parameters. Previously, some basic models have been developed and research has been carried out on the development of improved methods to provide accurate solutions. A major part of this study focuses on the effect of nozzle characterization on the flow behavior inside the gas solid riser. In reality, rectangular nozzles are used to generate liquid spray jets due to their high momentum conservation and deep penetration characteristics. However, this study provides a systematic work on the effect of nozzle aspect ratio on flow characteristics as well as the effect of fan angle. These are the two parameters that are easily controlled in the industrial applications. So an optimized value of these parameters will greatly serve the overall process efficiency.

The key factor governing the flow characteristics is the interaction mechanism between all three phases. The evaporation process is purely dependant on the heat transfer mechanism. The heat transfer between the solid and gas is negligible as both are maintained at same temperature in gas-solids suspensions. The heat transfer mode between the gas and liquid is relatively less significant when compared to the heat transfer mode between the solids and liquid droplets because the density of the solids is much higher than the gas density, hence the solids can provide much sustained heat transfer than gas phase. Therefore, it is very necessary to develop basic understanding of the physical interaction mechanism between solid and liquid phase. The physical mechanism is very complex in the presence of strong heterogeneous phase interaction mechanism. Solving this complex yet very challenging mechanism may lay down very pioneering steps in the development of efficient energy conversion methods.

1.3 Statement of the Problem

Single phase gas jets as well as two phase spray jets will be experimentally studied to compare the entrainment of the surrounding medium. In order to simplify the problem, both jets will be studied from a circular nozzle in submerged flow condition with room air as secondary medium. Mass of the surrounding air entrained inside the jet will be related to the mass of oxygen present inside the jet. Temperature and velocity profiles will also be monitored during the study. Entrainment in the presence of the solids can be studied numerically.

Effect of the aspect ratio of the rectangular nozzle will be studied both experimentally and numerically. A rectangular test section will be simulated with a circulating gas-solids flow. Rectangular nozzles with different aspect ratios are simulated to produce liquid nitrogen jets perpendicular to the gas-solids flow. Flow field structures will be compared. Similar studies will be carried out to investigate the effect of fan angle of rectangular nozzle.

An experimental system will be set up to study the effect of very hot solid particle falling over the water surface. The mono-sized particles will be generated using an arc generation system. During these experiments, different modes of type II Leidenfrost collision will be identified. Temperature profiles as well as the velocity measurements will be monitored with the help of experimental system. This information will then be employed to model the simple mechanistic collision mechanism between solid particle and liquid droplets at very high temperature difference between the two. Parametric study will be performed to study the effect of the particle temperature and particle velocity on the heat transfer mechanism.

1.4 Objectives of the Study

This study will be divided into three parts. Although, these three parts will be studied separately, it is important to note that there is a strong linkage between the three parts. In the first part, entrainments capabilities of two phase jets will be explored with respect to the similarity criterion, entrainment velocities, entrainment momentum ratio and evaporation rate along the jet trajectory. The study will comprise the experimental investigation of single phase-isothermal jet, single phase non-isothermal jet and two phase spray jet. Establishment of the similarity co-relations will be the very fist objective of the first part of this study and if proved, it will lay down the foundation for the development of mechanistic model for data analysis of the experiments.

In the second part, the objective is to obtain quantitative answers to the optimized nozzle parameters for effective and desired flow characteristics. Three-dimensional numerical study will be performed to systematically study the effect of aspect ratio of rectangular nozzle on flow characteristic. Complete flow information such as, spray penetration, spray deflection, solids concentration, gas temperature profiles as well as evaporation rate along the jet trajectory will be obtained and analyzed. The focus will be to find the optimum value of the nozzle aspect ratio. Similarly, the other controlling parameter of industrial nozzles i.e., nozzle fan angel will be studied with the same objective. In this case, the uniform evaporation rate will be the deterministic parameter for the choice of optimum value. Rectangular cross-section of domain will be used where the geometry will be such chosen that its effect on the flow is negligible.

The third part of this study will focus on the interaction mechanism between the small solid particle and large liquid surface. Experiments will be conducted with the objective of identifying different modes of heat transfer. The information will be used to develop basic mechanistic models which will incorporate all the basic important physics of the interaction mechanism. The models will be based on the heat and mass transfer balances between different phases. The models will be employed to provide basic parametric study on some governing parameters such as the initial temperature of the particle or initial velocity of the particle. The basic elements of this study will be to utilize experimental methods, numerical techniques and mechanistic modeling to answer complex questions regarding the flow behavior and interaction mechanisms of three phase flow structures. Upon successful completion of this study, it will provide basic fundamental information which will formulate the advance knowledge in this field.

CHAPTER 2

GAS ENTRAINMENT IN AN EVAPORATING SPRAY JET

2.1 Introduction

Rapidly evaporating liquid spray jets in gas solid suspensions are characterized by strong three phase interactions with momentum, heat and mass transfer across phase boundaries. This process occurs in many industrial applications such as fluidized catalytic cracking (FCC) of petroleum refinery, condensed mode operation of polyethylene synthesis, spray-assisted coal gasification, as well as environmental cleaning of suspended particulate by wet scrubbing. In all such applications, it is desirable to have a uniform evaporation of liquid spray jet within the jet boundaries which in turn depends on the homogenous collision between solids and droplets. In order to achieve this goal, it is essential to know the entrained solids, spray jet coverage and penetration into the gas-solids suspensions.

The entrainment characteristics and flow similarity of single-phase jets have been extensively studied [1]. For non-conventional single-phase jets such as a plunging jet to a liquid surface and plasma jets, the air entrainment, temperature and velocity similarities have also been investigated [2-4]. For two-phase non-evaporating swirling jets, the entrainment is greatly suppressed for a two-phase jet as compared to single-phase jets [5]. For a cross-flow spray jet without evaporation, the ratio of the cross-wind speed to the induced air speed governs the movements of the spray droplets. The flow at a high ratio may even diminish the entrainment [6]. The entrainment rates of reacting/non-reacting jets were compared using the mass balance

technique as well as by a velocity field measurement using Particle Image Velocimeter (PIV) [7]. However, neither temperature nor concentration measurements were reported in their study. Studies on the entrainment of two-phase (gas-solid) surrounding media by a gas jet have been reported [8-10]. The entrainment velocity is found to decrease with the distance from nozzle, increase with the nozzle velocity and decrease with the solid loadings.

This study aims to address the important subject that has never been studied before: evaporation effect of droplets on gas entrainment of a spray jet. In this study, an experimental study is performed of a liquid nitrogen spray into the room air. Direct measurements of the oxygen concentration and droplet velocity in the spray region are obtained, based on which the air entrainment and spray evaporation rate are calculated. Due to the difficulties in premixing tracer particles into the liquid nitrogen system and from the direct contact of droplets with thermocouples, the direct measurements of gas velocity and gas temperature in the liquid nitrogen spray region cannot be obtained via LDV and thermocouple measurements. The limited size of spray nozzle also prevents an accurate measurement of radial profile in the near field of the liquid nitrogen spray jet. Alternatively it is assumed that the dimensionless distribution of gas temperature in the spray region is the same as that of concentration; and the dimensionless gas velocity can be represented by that in the absence of spray. These assumptions have been partially validated from the comparison of direct measurements of oxygen concentration with and without spray, from the numerical simulation of liquid nitrogen spray in a co-axial gas-solid flow

[11], and from the comparison of temperature and concentration measurements in the absence of spray.

Besides the measurements, a parametric model has been developed to provide the theoretical basis of data analysis, which is to solve for three coupled unknowns: gas entrainment velocity, spray evaporation rate, and centerline gas velocity. The measurement and modeling methodology, in principle, do not require the use of any similarity laws. However, to simplify the data analysis, as suggested in measurements and previous numerical simulations [11] within the tolerance range, the similarity is used as an engineering approximation.

2.2 Experimental System for Entrainment Experiment

There are two experimental setups in this study. One is for the gas entrainment with a cold nitrogen gas jet, which is to provide a comparison base for the study with spray, and the other is for the gas entrainment with a liquid nitrogen spray. Figure 2.1 shows a combined schematic diagram of both experimental setups. When valve A is open and valve B is closed, a very cold jet of nitrogen gas (at approximately the temperature of liquid nitrogen) is generated from a compressed nitrogen gas container by passing through a heat exchanger submerged in liquid nitrogen. The cold gas jet is then injected into the stagnant room air. Conversely, if valve A is closed and valve B is open, Figure 1(a) then represents the schematics of the experimental apparatus for evaporating spray jets, where the sprays of liquid nitrogen are generated from a pressure-controlled spray generation system (25-liter, Brymill Cryogenic). This system hence is capable of producing a sustained spray jet of liquid nitrogen. The

sustainability depends on the size of nozzle and the operation pressure inside the liquid nitrogen tank. In this study, a sustained liquid nitrogen spray with a constant flow rate is obtained for approximately 40 minutes. Figure 2.2 shows the detailed structure of the spray nozzle, which consists of a small centerline tube (1 mm in diameter) for atomization and a coaxial and thermally-insulated tube (5 mm in diameter) for spray confinement and smoothing. This nozzle structure helps to generate a liquid nitrogen spray with a reasonably large initial spray diameter, which is needed for the measurements of spray radial profiles near the spray nozzle.

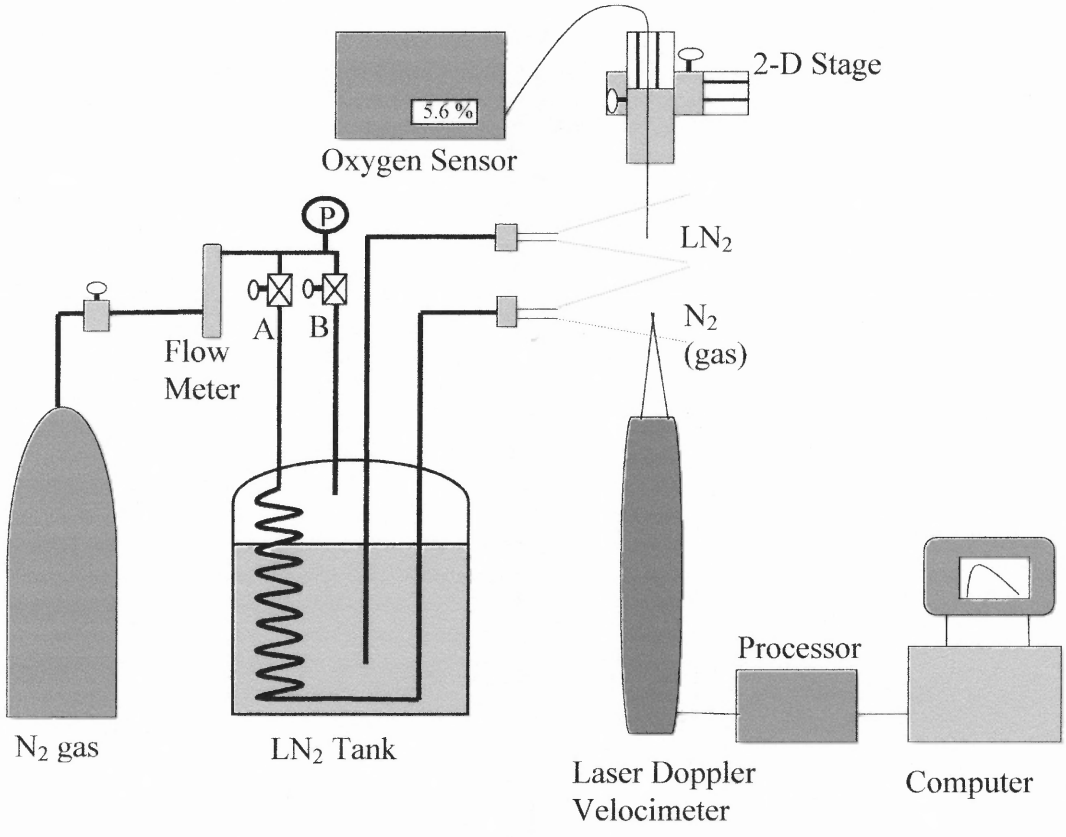

Figure 2.1 Experimental setup for cold Nitrogen gas jet (near LN2 temperature).

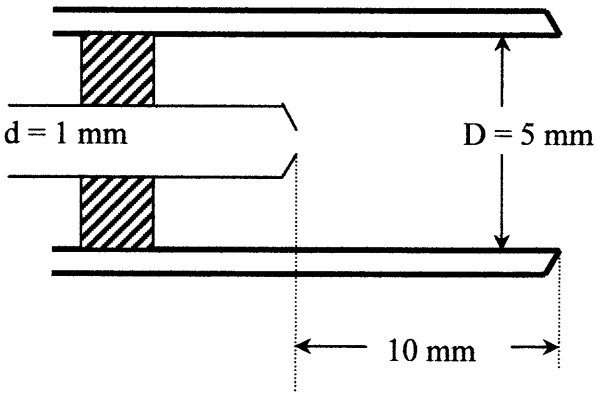

Figure 2.2 Nozzle structure for the two-phase spray jet.

An *in-situ* oxygen concentration analyzer (CE0123, Oxigraf) with a thermal compensation and control mechanism is specially designed for measurements of oxygen concentration at extremely low temperatures. The oxygen sensor probe (1.25 mm orifice) is mounted on a precision 3-D stage. This oxygen analyzer is capable of measuring the oxygen concentration with an accuracy of 0.1%, and the measurements are independent of sample pressure, gas temperature and other gases such as CO_2 or H_2O. The temperature profiles are obtained using a tiny Type-J thermocouple (0.5 mm O.D.) connected to a PC-based temperature measurement system. A Laser Doppler Velocimeter (Flowlite 1-D, Dantec) is used for the measurement of spray jetting velocity as well as axial distributions of droplet velocity along the spray jet. The interrogation region in the LDV measurement is an intersection of two laser beams of waist diameter of 1 mm each. A PC-based precision balance (SV-30, Acculab) is employed to measure the mass flow rate of the spray injection. The atomization characteristics of liquid nitrogen sprays are pre-calibrated using a Phase Doppler Particle Anemometer (PDPA 58N70, Dantec) [12]. The averaged initial

droplet size from the spray nozzle is about 160 μm. For nitrogen gas jet, the jetting velocity is obtained from the flow rate measurement using a rotary flow meter.

2.3 Theoretical Basis and Methodology

The modeling approach takes the advantages of the fact that, in a free spray jet of liquid nitrogen injected into the air, liquid nitrogen evaporation does not contribute to the amount of oxygen in the spray region, and all oxygen found in the spray region is solely from the jet-induced entrainment. Hence the air entrainment between any two jet cross-sections is proportional to the difference of oxygen mass flows at these two cross-sections. The proportionality depends on the ambient oxygen concentration. In the room air with the oxygen concentration of 21%, this proportionality is 4.76. In the following section, first the general equations and methodology of this model is described, and then the discussion is extended to special applications where jet flow similarities hold. The introduction of flow similarity can greatly reduce both the complicity in equation solution processes and the demand of extensive measurements in the spray region. As shown from measurements in the section of results and discussion, it is reasonable to assume flow similarities in this study.

2.3.1 Governing Equations

Consider an arbitrary jet cross-section segment shown in Figure 2.3. The oxygen mass flow rate J_{O_2} across any jet cross-section is given by

$$J_{O_2} = \int_0^\infty 2\pi r \rho C U dr \tag{2.1}$$

where ρ is the overall density of all gaseous species, C is the oxygen concentration, and U is the gas velocity. Assuming that the overall gas follows the ideal gas law and the ambient pressure and the gas constant remain unchanged with the liquid nitrogen evaporation, the density is given by

$$\rho = \frac{P}{RT} \tag{2.2}$$

where P is the ambient pressure, R is the gas constant and T is the temperature of ambient air.

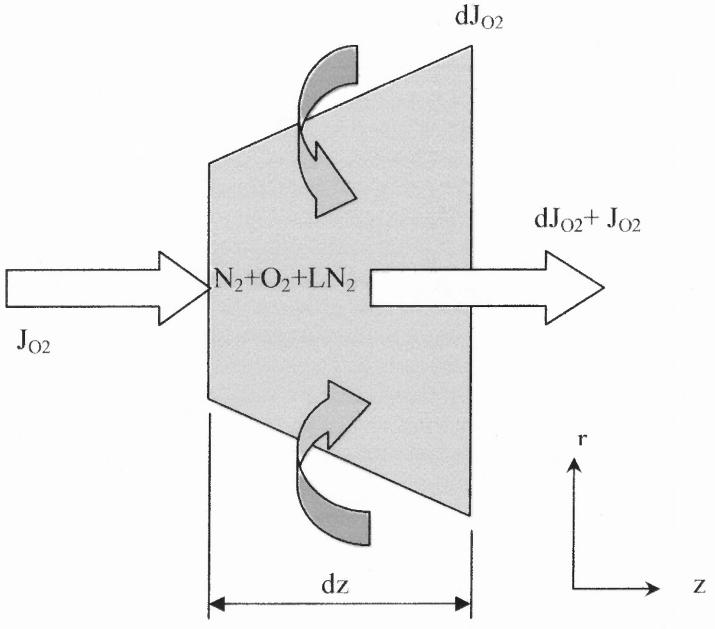

Figure 2.3 Gas (oxygen) entrainment from mass flow balance.

Hence, the oxygen mass flow rate, which is a function of axial location itself, depends solely on the radial distribution of the velocity, concentration and temperature. From the mass balance of oxygen, the radial component of the air entrainment velocity U_e is thus given by

$$U_e \approx \frac{1}{2\pi b C_\infty \rho_\infty}\left(\frac{dJ_{O_2}}{dz}\right) \tag{2.3}$$

where z is the distance from the nozzle exit and b is the jet width. The heat convection of gas phase $\dot{E}$ at any jet cross-section is calculated by

$$\dot{E} = \int_0^\infty 2\pi r \rho U c_p T dr \tag{2.4}$$

where c_p is the specific heat at constant pressure of nitrogen. Thus, the energy balance over a jet spray segment with a thickness of Δz can be expressed by

$$\dot{E} + 2\pi b U_e \rho_\infty c_p T_\infty \Delta z - L\Gamma \pi b^2 \Delta z \approx \dot{E} + \frac{d\dot{E}}{dz}\Delta z \tag{2.5}$$

where L is the specific latent heat, and Γ is the rate of mass evaporated of liquid nitrogen per unit volume. Equation (2.5) yields the following equation for the estimation of Γ.

$$\Gamma \approx \frac{1}{L\pi b^2}\left(2\pi b U_e \rho_\infty c_p T_\infty - \frac{d\dot{E}}{dz}\right) \tag{2.6}$$

Another important physical law is the momentum conservation. For a horizontal spray jet, the total momentum along the jet direction is conserved at any jet cross-section. For simplicity, the Archimedean effect on the jet deflection and jet asymmetry is neglected, as observed and partially validated from experiments. It is assumed that the droplet velocity only varies along the jetting direction. Hence, the jet-directional momentum conservation of this two-phase flow at any jet cross-section is given by

$$J_{mj} U_j = \int_0^\infty 2\pi r \rho U^2 dr + J_d U_d \tag{2.7}$$

where J_{mj} is the total jetting mass flow rate at the nozzle exit; U_j is the jetting velocity at the nozzle exit; U_d is the cross-section averaged droplet velocity; and J_d is the cross-section averaged droplet mass flow rate, which can be linked to the spray evaporation rate per unit volume by

$$J_d \approx J_{dj} - \int_0^z \pi b^2 \Gamma dz \tag{2.8}$$

where J_{dj} is the jetting liquid mass flow rate at the nozzle exit. Based on Equation (2.8), the evaporation length L_e can be defined and calculated from the mass balance of liquid nitrogen as

$$J_{dj} \approx \int_0^{L_e} \pi b^2 \Gamma dz \tag{2.9}$$

Based on the three independent governing equations, i.e., Equation (2.3), Equation (2.6) and Equation (2.7), respectively representing the mass, heat and momentum conservation, three independent variables can be solved. In this study, the distributions of oxygen concentration, droplet velocity, and gas temperature in the spray region can be determined, either from the direct measurements or based on the analogy between temperature and concentration profiles. Thus, in principle, the three unknowns, namely the gas entrainment velocity U_e, spray evaporation rate Γ, and the averaged gas velocity U, can be obtained by solving the coupled governing equations.

2.3.2 Solution Procedures with Flow Similarity

In jet flow applications, when flow similarities exist, the introduction of flow similarity can significantly simplify the equation solution processes as well as reduce the demand of extensive measurements in spray region. With the flow similarity, it is convenient to express the governing equations with dimensionless variables. Here, it is defined as

$$r^* = \frac{r}{b}, \qquad C^* = \frac{C_\infty - C}{C_\infty - C_0}$$
$$U^* = \frac{U_\infty - U}{U_\infty - U_0}, \qquad T^* = \frac{T_\infty - T}{T_\infty - T_0} \tag{2.10}$$

where b is the jet width, r is the radial distance from the center of the jet, T is the temperature inside the jet and the subscripts of 0 and ∞ denote, respectively, the centerline and ambient locations, and superscript * stands for the dimensionless quantity.

Conceptually, the jet boundaries of velocity, temperature and concentration are different [1]. There exists an analogy between the profiles of temperature and concentration so that the jet widths of temperature profile and concentration profile are about the same whereas the jet width of velocity profile is narrower than those of temperature and concentration profiles [1]. In a spray jet with strong vaporization of droplets, the effect of droplet vaporization minimizes the difference of these jet widths [12]. To simplify the analysis of spray jets with strong vaporization, the jet boundary is assumed to be the same for the gas velocity, temperature and concentration. This assumption is partially validated in the measurements, as shown in Figure 2.5.

Substituting Equation (2.2) and Equation (2.10) into Equation (2.1) and noting that, for a free jet, $U_\infty = 0$,

$$J_{O_2} \approx 2\pi b^2 \frac{P}{R} U_0 \left(\frac{r^* U^* \{C_\infty - (C_\infty - C_0)C^*\}}{T_\infty - (T_\infty - T_0)T^*} \right) dr^* \tag{2.11}$$

where P, R, U_0, C_0, C_∞, T_0 or T_∞ is either a constant or a function of axial location (z) only; and the jet boundary b is defined based on the dimensionless radial profiles of concentration. Specifically, the jet widths are measured using the interpolation on the dimensionless concentration profiles using the 5% cut-off criterion. Theoretically, a more stringent criterion of 1% can be applied to better define the jet boundary. However, considering the jet-induced fluctuations and uncertainties in the concentration measurements, the 5% cut-off criterion is preferred and used throughout this study.

Similarly the heat convection of gas phase $\dot{E}$ at any jet cross-section is expressed, according to Equation (2.4) and Equation (2.3), by

$$\dot{E} \approx 2\pi b^2 c_p \frac{P}{R} U_0 \int_0^1 r^* U^* dr^* \tag{2.12}$$

In this study, the jet boundary b and oxygen concentration distributions are directly obtained from the oxygen concentration measurements, which yield both r^* and C^*. Due to the collision of liquid nitrogen droplets with the thermocouple, the gas temperature is difficult to be directly measured in the spray region [13]. The dimensionless profile of gas temperature in the spray region is assumed to be the same as that of oxygen concentration, i.e., $T^* = C^*$. This analogy is true for a cold nitrogen jet (at a jetting temperature slightly above the liquid nitrogen temperature)

into the room air, based on the direct measurements of oxygen concentration and temperature in the jet region as shown in Figure 2.6. In a spray region, the effect of strong evaporation of liquid nitrogen droplets leads to a lowered gas temperature as well as a diluted oxygen concentration simultaneously. Hence the assumption of similar gas temperature and gas concentration profiles in the presence of strong evaporation is reasonable. This assumption is partially validated by a numerical study of the liquid nitrogen spray jets in concurrent dilute gas-solid flows [12]. The centerline gas temperature in the liquid nitrogen spray is found to be very close to that of liquid nitrogen temperature [12], so that $T_0 \approx T_d$. The droplet velocity U_d is determined directly from the LDV measurements.

Difficulty also rises to the determination of gas velocity profiles in the spray region. Firstly, the only naturally-available "tracers" in a liquid nitrogen spray are the droplets of liquid nitrogen. It is difficult to add or premix other tracers into the liquid nitrogen spray, due to the extremely-low temperature of liquid nitrogen as well as the limited size of liquid nitrogen nozzle system. Secondly, the dense population of droplets in the near field of spray jet and the poly-atomization in liquid nitrogen droplets make the LDV measurements inapplicable to the determination of gas velocity in the spray region. In addition, the limited size of spray nozzle also prevents an accurate measurement of radial profile in the near field of the liquid nitrogen spray jet. Hence, in this study, it is assumed that the dimensionless profile of gas velocity in the spray jet is the same as that in the cold gas jet, as partially validated by the previous numerical investigation of liquids nitrogen sprays in gas-solids suspensions [11]. However, the centerline gas velocity is still unknown, which is to be solved

along with the gas entrainment velocity and the evaporation rate from the governing equations. Table 2.1 lists the parameters of nitrogen gas jets and liquid nitrogen spray jet with a round nozzle in this study. All jets are injected into the stagnant room air. The room air temperature is maintained at 297 K.

Table 2.1 Parameters of gas and spray jets

Jet type	Jet temperature (K)	Nozzle diameter (mm)	Jetting velocity (m/s)	Jetting mass flow rate (g/s)	Jet Reynolds Number
nitrogen gas jet (isothermal)	291	5	30	0.64	10,700
nitrogen gas jet (non-isothermal)	118	5	26	1.76	49,000
liquid nitrogen spray	74	5	23	3.64	570,000

2.4 Results and Discussion

2.4.1 Validation of the Experimental System and Measurement Methods

It is important to validate the experimental approaches on the jet measurements. In order to do that, gaseous jets of nitrogen in the stagnant air are studied first. The dimensionless concentrations are plotted against the well-known correlation $C^*=1-r^{*3/2}$ [1], as shown in Figure 2.4. The experimental data matches the above mentioned curve very well. The comparison of measured jet boundary expansion and predictions from Abramovich's jet model [1] $b/z = 0.11(1+\rho_\infty/\rho_j)$ is shown in Figure 2.5. The difference can be caused by several different factors, including the effect of turbulence and the effect of nozzle structure (such as shape of nozzle tip).

Another factor is the difference in definition of b. In the Abramovich's model, b is defined with 1% cut-off whereas in this study it is defined from the dimensionless concentration profiles with 5% cut-off. Given the influence of these factors, the experimental data for the boundary expansion of both isothermal and cold nitrogen jets are regarded quite close to the Abramovich's relation. Hence, the comparison between the measurements and well-known correlations in Figure 2.5 and Figure 2.6 validates the current experimental system and measurement methods.

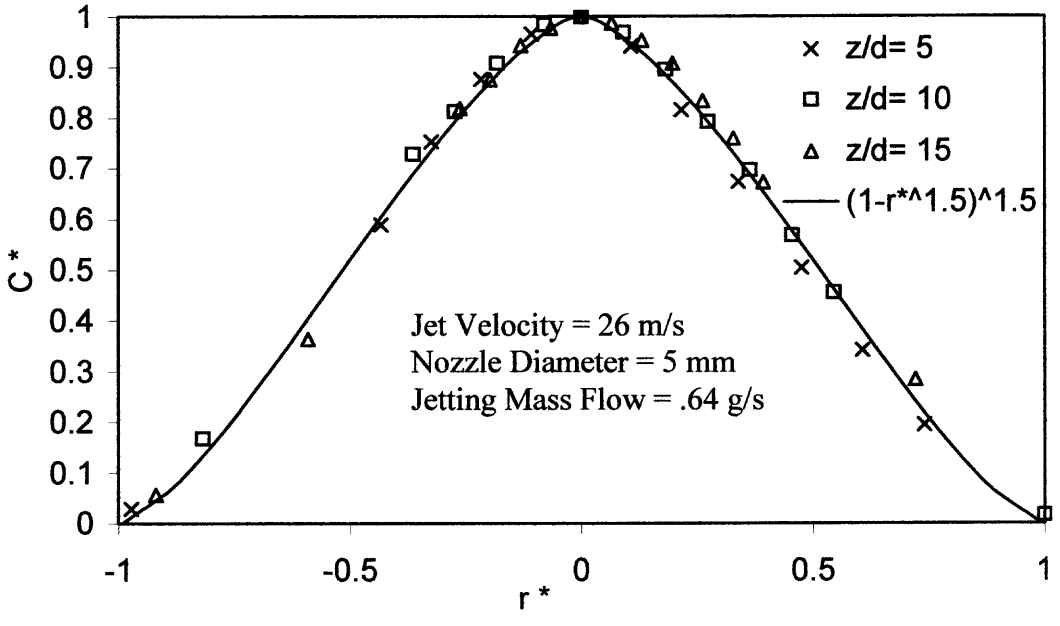

Figure 2.4 Dimensionless oxygen concentration radial profiles (with theoretical comparison) in an isothermal nitrogen gas jet.

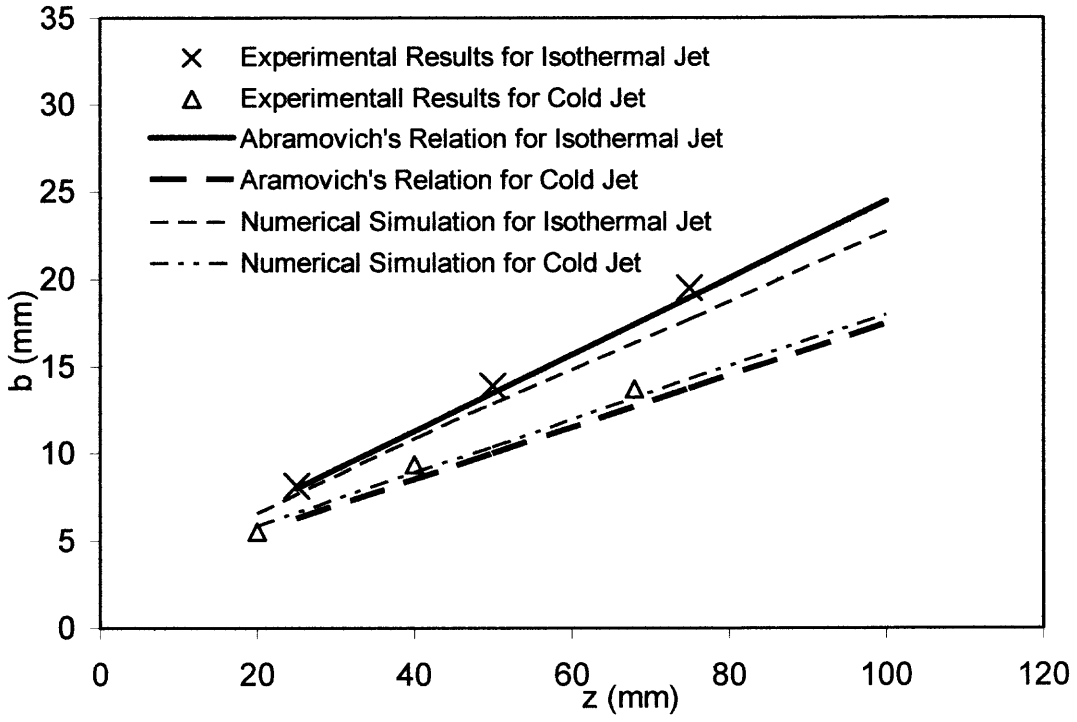

Figure 2.5 Jet expansions (with theoretical comparison) of nitrogen gas jets.

2.4.2 Radial Distributions and Similarity

According to Equations (2.3) and (2.6), in order to obtain the air entrainment and spray evaporation rate, one must predetermine the oxygen mass flow, which calls for the information on the radial distributions of oxygen concentration, gas velocity and gas temperature at any spray jet cross-sections. While the oxygen concentration profile can be directly measured using the oxygen probe and analyzer, the direct measurements of local gas temperature and velocity in the presence of fast-moving and evaporating droplets turn out to be extremely difficult, if not impossible, by use of the thermocouple and LDV measurement techniques. The difficulties arise from the interference with the second phase, i.e., the droplet phase. Due to the direct collision of droplets with the thermocouple in the spray region, the measured

temperature represents only a mixed temperature of gas and liquids rather than the temperature of gas [13]. In the particle-free spray region where there are no tracing particles representing the gas phase, LDV measures only the velocities of droplets but not the velocity of the gas. Hence, an alternative means for determining the radial distributions of gas temperature and velocity is adapted in this study.

According to turbulent jet theory [1], the radial distribution of dimensionless temperature is analogous to that of dimensionless concentration, which means the overlap of the dimensionless concentration and the temperature profiles. This analogy is validated in the experimental study, as shown in Figure 2.6. It may be reasonable to assume that, in a spray jet, the radial distribution of the dimensionless temperature is still the same as that of the dimensionless concentration in a spray jet. Therefore, based on the direct measurements of oxygen concentration with a liquid nitrogen spray, both concentration and temperature radial profiles can be determined.

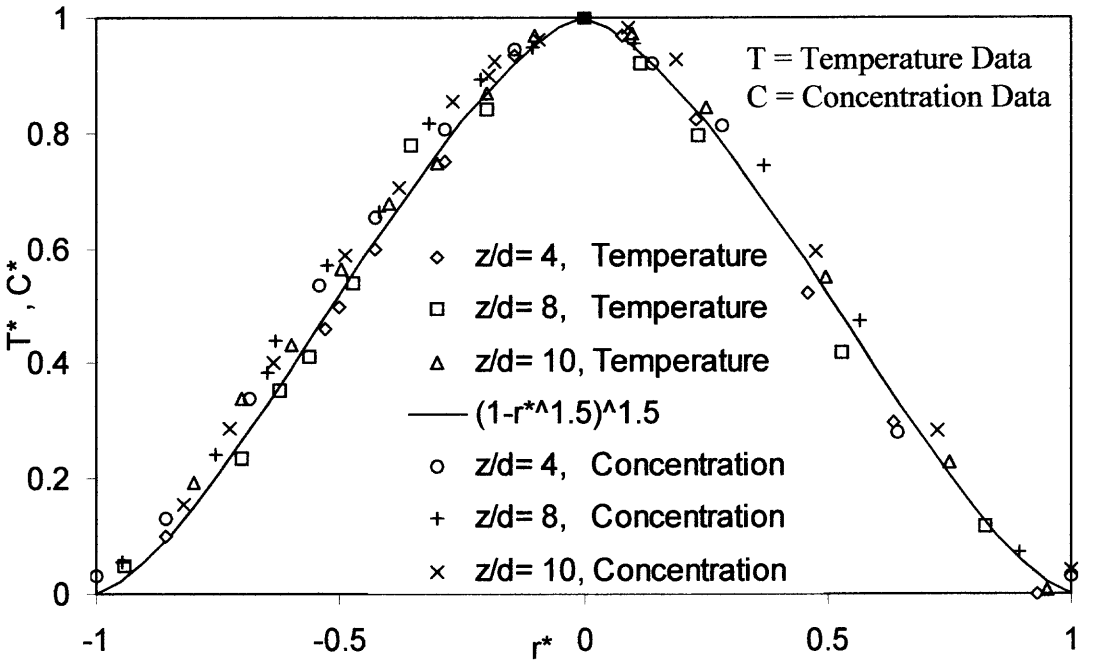

Figure 2.6 Dimensionless profiles of temperature and concentration in gas jets.

A recent numerical study of a liquid nitrogen spray in a dilute gas-solid suspension pipe flow suggested that the jet similarities, in the presence of evaporating liquid nitrogen droplets and dilute solid particles, is still quite similar to those of single-phase jets [11]. This result strongly supports the assumption that the dimensionless radial distribution of gas velocity in the liquid spray jet is the same as the dimensionless profile of gas velocity in the cold gas jet.

2.4.3 Air Entrainment Rate

Figure 2.7 shows the dimensionless profiles of oxygen concentration for a two-phase spray jet, which can be expressed by a simple semi-empirical correlation $C^* = \exp(-5r^{*2})$. The similarity curve in Figure 2.7 appears somewhat skewed

towards the center of the jet as compared to that of single phase jets. This difference may be caused by the effect of radial profiles of droplet momentum and droplet evaporation rate that are not necessarily following the flow similarities. In this study, the similarity holds valid for a jet axial distance range up to z/d of 20.

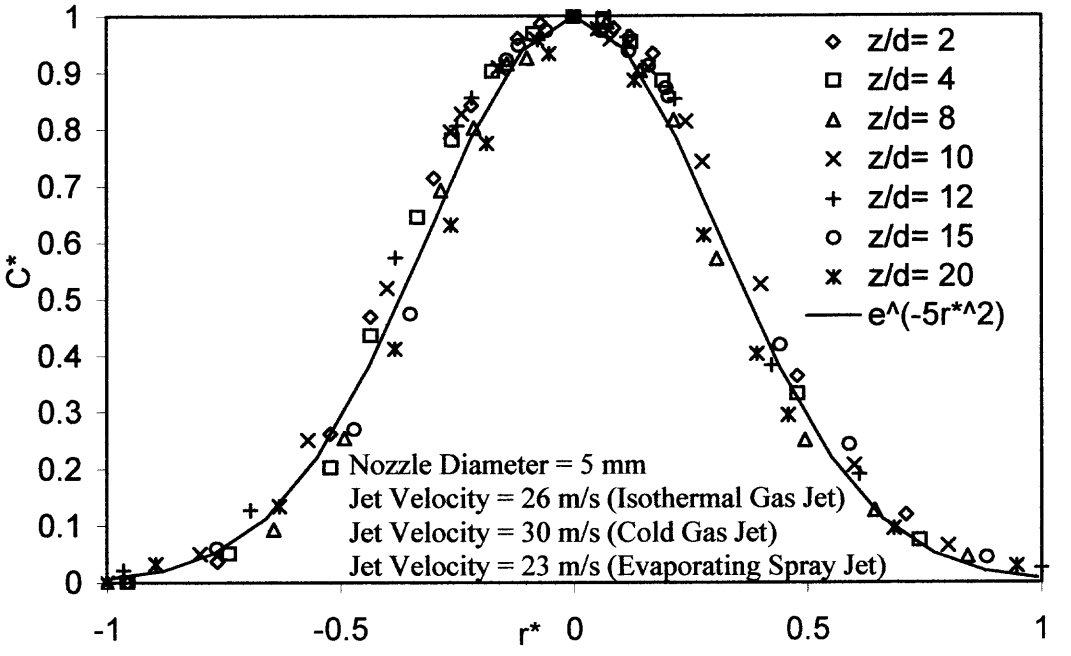

Figure 2.7 Dimensionless oxygen concentration profiles in a liquid-nitrogen spray jet.

2.4.4 Effect of Evaporation on Jet Expansion

Figure 2.8 shows the corresponding jet boundary that is determined based on oxygen concentration profiles. The results suggest that the isothermal gas jet has the least boundary expansion while the spray jet has the maximum jet boundary expansion, especially in the initial stage of jetting where the most evaporation occurs.

2.4.5 Entrainment Velocity

The comparison of gas centerline velocity of a spray jet and the theoretical curve of a gas jet at the same injection velocity is shown in Figure 2.9. The quick decay of the centerline velocity in the initial part of the gas jet shows that the jet momentum is not able to maintain the velocity for a longer distance after exiting from the nozzle. For the spray jet, however, the decrease in the centerline gas velocity is slower. This slower decay is due to the greater inertia of droplets as well as due to the vapor generation from droplet evaporation that not only helps to sustain the gas phase velocity but also expand the jet boundary. The air entrainment velocities of gas jet and spray jet at the same jet velocity are found to be comparable, as shown in Figure 2.10. However, due to the different injecting momenta between the two jets at the same jetting velocity, a more meaningful comparison should be based on the entrainment per unit injecting momentum. Due to the much higher density of droplets than the air density, entrainment per unit injecting momentum in the spray jets is at least one order of magnitude less than that in gas jets, as shown in Figure 2.11, which indicates that the rapidly evaporating spray jets have less capabilities of air entrainment than the gas jets at the same jet velocity.

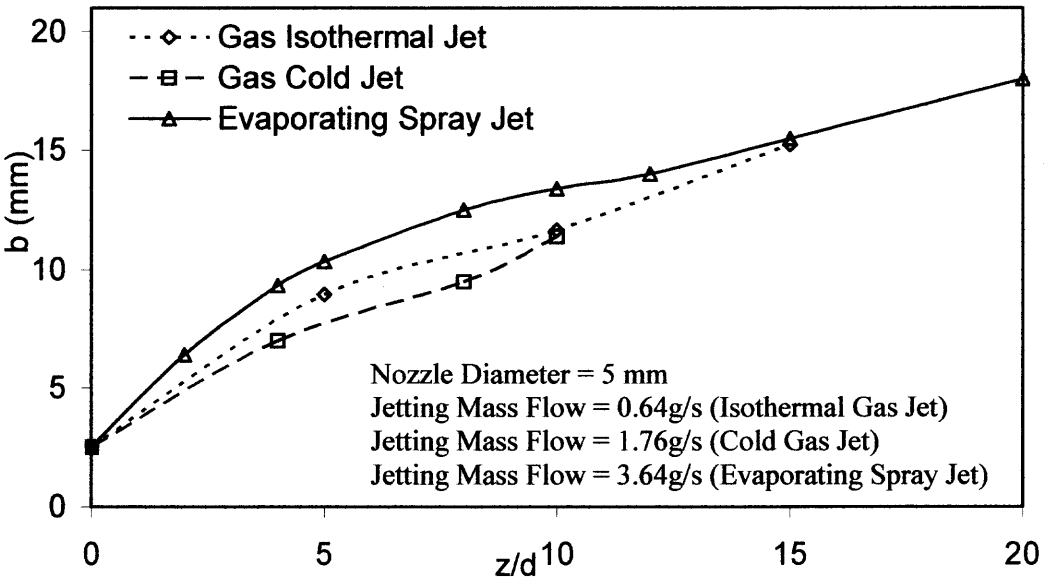

Figure 2.8 Comparisons of jet boundary expansions between gas jets and spray jets.

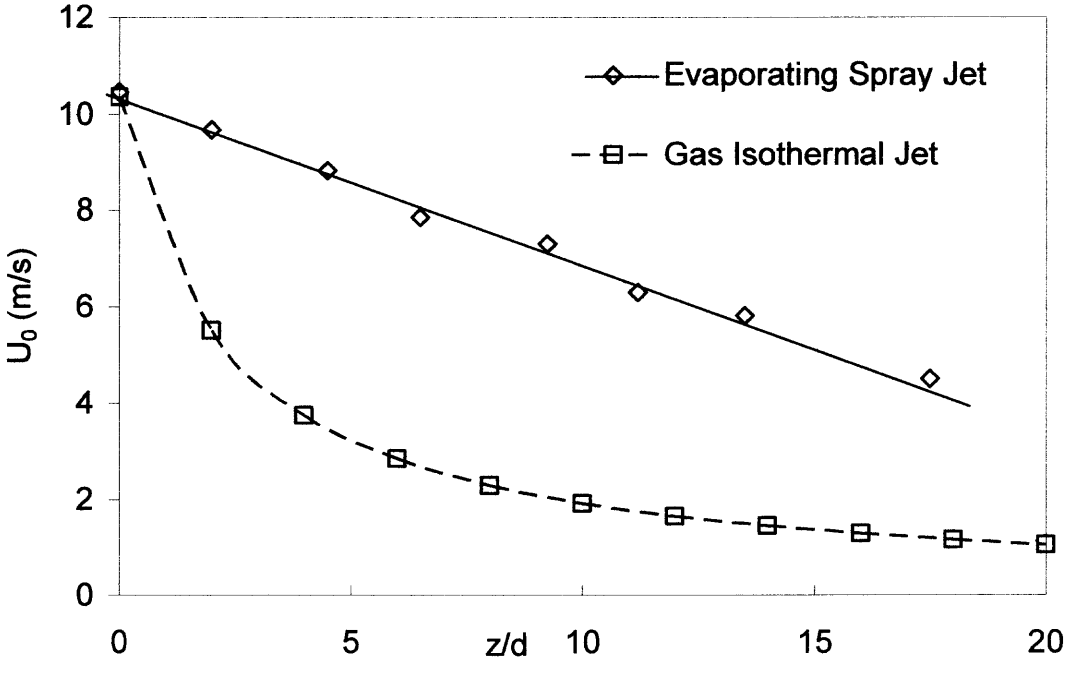

Figure 2.9 Comparison of centerline velocity between gas jets and spray jets.

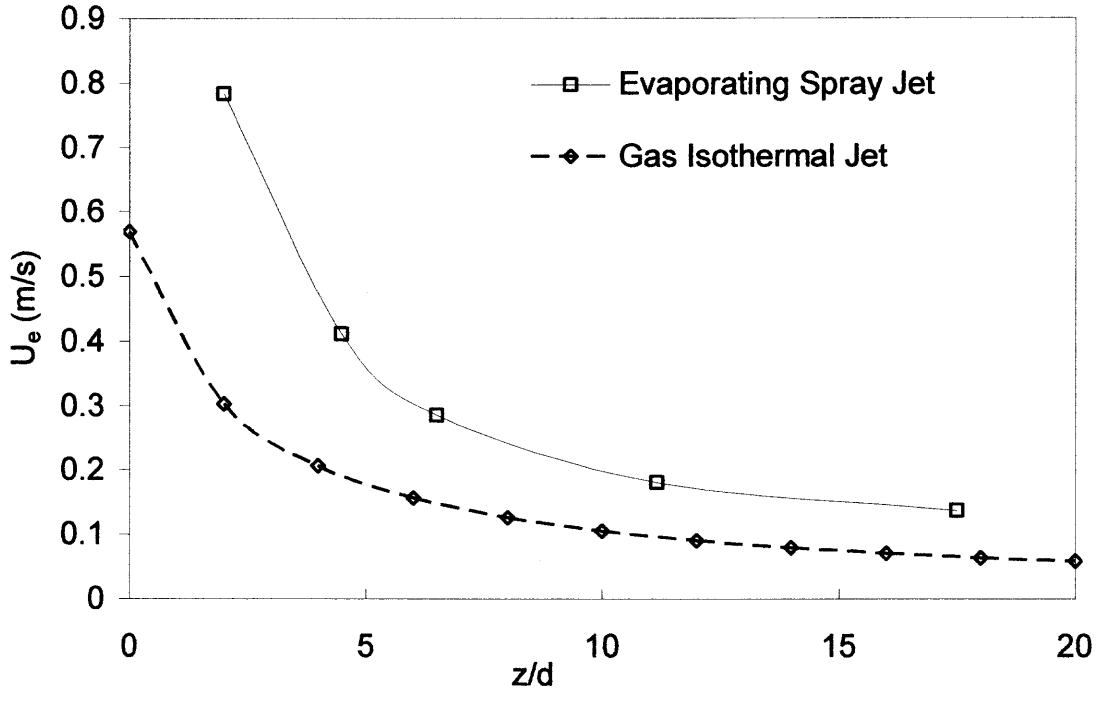

Figure 2.10 Comparison of entrainment velocity between gas jets and spray jets.

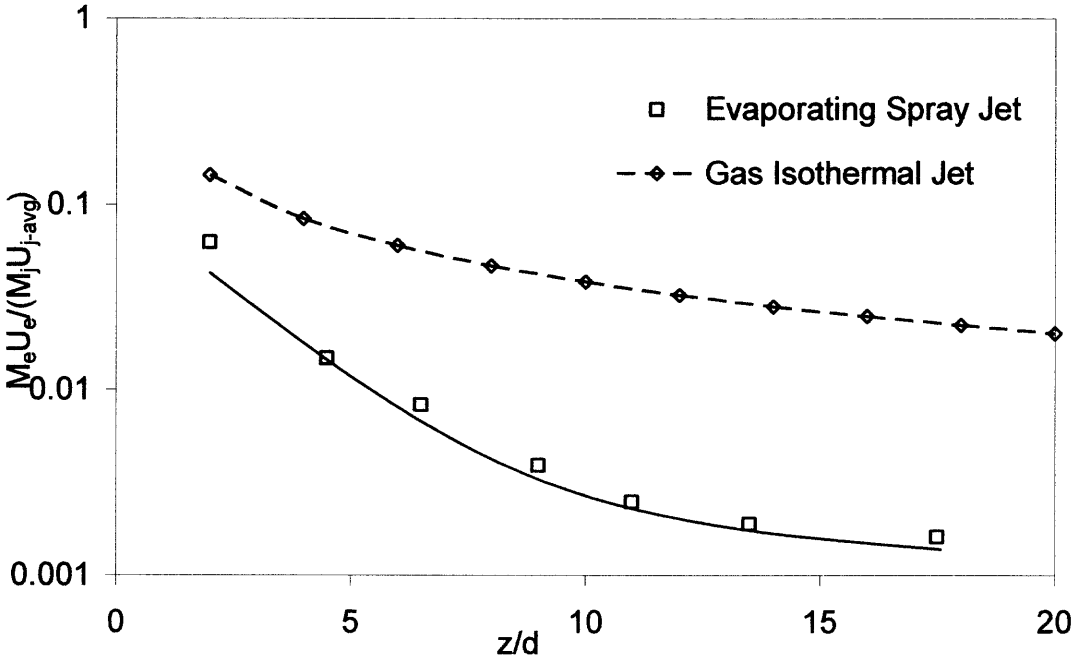

Figure 2.11 Comparison of entrained momentum between gas jets and spray jets.

2.4.6 Evaporation Rate of Spray Jet

One of the objectives of this study is to estimate the evaporation rate. This is achieved by checking the energy balance at any segment of the spray jet, as expressed by Equation (2.6). The axial distribution of the evaporating rate is shown in Figure 2.12. A higher evaporation rate in the initial region of the spray jet is due to the higher air entrainment that brings in more thermal energy for the droplet evaporation. For the case in current study, as much as 80% of the injected liquid is evaporated within the range of z/d of 6. However, due to the non-uniform droplet size distribution and non-uniform jetting velocity distribution, some liquid nitrogen droplets are found to travel much further along the jet. On the average, a spray penetration length (or evaporation length) can be defined in a way that the integrated evaporation rate over that length equals the injected liquid mass flow rate, as shown in Equation (2.9).

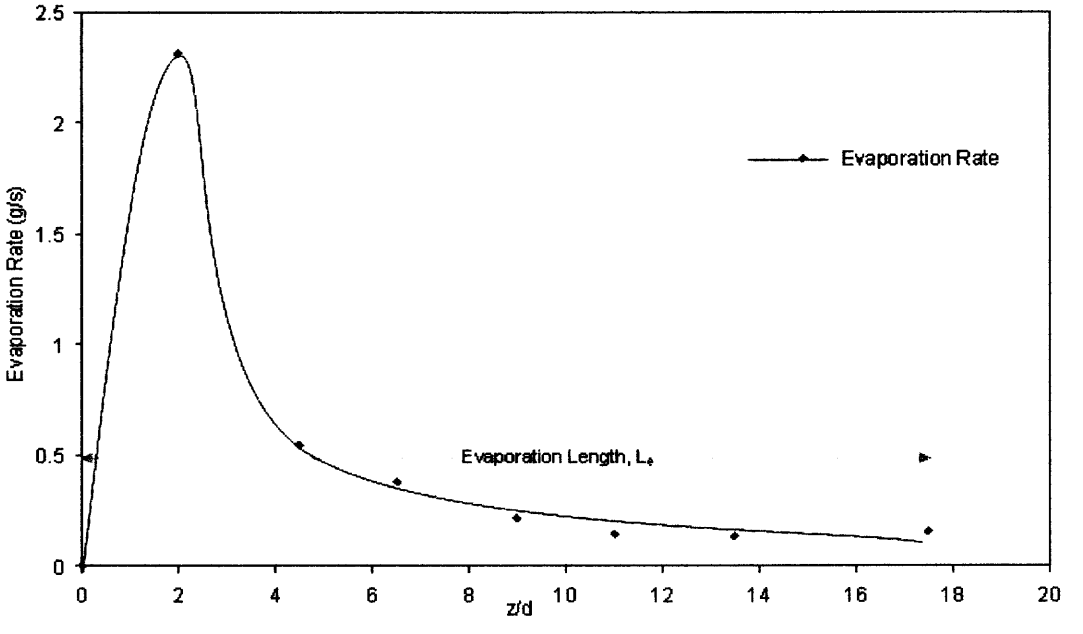

Figure 2.12 Axial distribution of evaporation rate in a liquid-nitrogen spray jet.

2.5 Conclusions

A direct measurement technique of gas entrainment in an evaporating jet has been developed. A parametric model has been developed to provide the theoretical basis of data analysis for the gas entrainment. The air entrainment characteristics of the liquid nitrogen spray jet injected into the stagnant room air is found to be quite different from those of the nitrogen gas jets at the same jet velocity from the same nozzle. The measurements of gas concentration distributions in the liquid nitrogen spray jets suggest the existence of jet similarity within most of the spray jet region. The measurements further shows that the concentration-based jet boundary is wider for the spray jets than that for the gas jets whereas the entrainment per unit injecting momentum in spray jet is much less than those in the gas jets. In addition, distributions of gas velocity on the centerline and evaporation rate are also obtained.

2.6 Future Study

2.6.1 Gas-Solids Entrainment in Circular Spray Jets with Cross-flow Effect

A more realistic entrainment study can be carried out for s spray jet from a circular nozzle in the cross flow of air. This will lay down the foundation for the cross flow experiment. This study will reveal whether the similarity holds in case of cross-flow or the deflection of spray jet destroys the similarity profiles of temperature, velocity and concentrations.

2.6.2 Gas-Solids Entrainment in Submerged Rectangular Spray Jets

Due to the difficulties in the measurement techniques in the presence of the solids, it is almost impossible to study the entrainment of solids in the spray jet experimentally. However, numerical simulation studies can be carried out to quantify the effect of solids entrainment on the spray structure. With the help of correct model, the entrainment of solids can be quantified with the help of 3-D simulations.

CHAPTER 3

EFFECT OF NOZZLE CHARACTERISTICS ON THE FLOW STRUCTURE OF EVAPORATING SPRAY JETS

3.1 Introduction

In principle, a horizontal and a vertical configuration of a rectangular flat nozzle should have different flow characteristics. To design an optimal nozzle for these applications may be somewhat complicated due to the fact that it is not possible to optimize all the governing characteristics of the spray jets for the same nozzle configuration. In FCC application, the rectangular nozzles are used due to their wide spread range and as well as their mass and momentum conservations are quite different than circular nozzles.

Hydrodynamics on single-phase jets is well known [14, 15]. For the two-phase jets, especially spray jets, reasonable understanding on jet or spray characteristics such as penetration length and evaporation rate has been achieved [16, 17]. Recently new attention has been paid to hydrodynamic behaviors of three-phase jets that have some significant industrial applications. An experimental study, using a sampling probe, for the flow mixing of liquid nitrogen spray in a preliminary industry-scaled FCC riser was reported [18]. An electrical capacitance tomography technology was developed to diagnose the flow patterns of evaporating liquid nitrogen jets into a dense phase fluidized bed [19]. The increase in solids loading is found to shorten the spray penetration [20, 26]. Parametrical models to investigate the coupling interactions of all three phases have been proposed [21, 22]. Numerical simulations on the three-phase spray jets have also been attempted [23-24]. However,

nearly all these studies are for the circular nozzle sprays. There is, however, very limited information available on the quantitative comparison between nozzles with different aspect ratios. Once using a rectangular nozzle, it is realized that the flow patterns could be significantly altered by the nozzle aspect ratio (for the same area of nozzle openness) or by the nozzle orientation.

3.2 Numerical Simulation Method

A detailed discussion on numerical simulation method can be found in a pervious paper [20]. However, only 2-D results were presented in that study. In this study, the code is modified to simulate 3-D flow structures. A set of key governing equations are summarized below.

3.2.1 Governing Equations of Gas-Solid Flow

It is assumed that the solids are mono dispersed without attrition. The gas phase is a mixture of air and nitrogen vapor where the air and nitrogen vapor have the same physical properties so that no gaseous species equations need to be solved. Hence, the governing equations of gas phase flow are given by

$$\frac{\partial}{\partial t}\left(\varepsilon_g \rho_g\right)+\nabla\cdot\left(\varepsilon_g \rho_g \vec{v}_g\right)=\Gamma \tag{3.1}$$

$$\frac{\partial}{\partial t}\left(\varepsilon_g \rho_g \vec{v}_g\right)+\nabla\cdot\left(\varepsilon_g \rho_g \vec{v}_g \vec{v}_g\right)=\nabla\cdot\bar{\bar{S}}_g+\varepsilon_g \rho_g \vec{g}-\vec{I}_{gs}-\vec{I}_{gd}+\Gamma\vec{v}_d \tag{3.2}$$

$$\varepsilon_g \rho_g C_{pg}\left(\frac{\partial T_g}{\partial t}+\vec{v}_g\cdot\nabla T_g\right)=-\nabla\cdot\vec{q}_g-H_{gs}-H_{gd}+\Gamma C_{pg} T_d \tag{3.3}$$

where the source terms include contributions not only from the mass generation but also from the momentum and energy transfer between gas and droplets. Similarly the equations for solid phase are given by

$$\frac{\partial}{\partial t}(\varepsilon_s \rho_s) + \nabla \cdot (\varepsilon_s \rho_s \vec{v}_s) = 0 \tag{3.4}$$

$$\frac{\partial}{\partial t}(\varepsilon_s \rho_s \vec{v}_s) + \nabla \cdot (\varepsilon_s \rho_s \vec{v}_s \vec{v}_s) = \nabla \cdot \bar{\bar{S}}_s + \varepsilon_s \rho_s \vec{g} + \vec{I}_{gs} - \vec{I}_{sd} \tag{3.5}$$

$$\varepsilon_s \rho_s C_{ps} \left(\frac{\partial T_s}{\partial t} + \vec{v}_s \cdot \nabla T_s \right) = -\nabla \cdot \vec{q}_s + H_{gs} - H_{sd} \tag{3.6}$$

where the additional source terms account for effects due to droplet-solid collisions.

3.2.2 Turbulence Model

In a turbulent particulate multi-phase flow, the particles are dispersed through turbulent flow fluctuations. The addition of particles can enhance or reduce the flow turbulence, affecting transport behavior of both particle and flow phases. With evaporating droplets, the turbulence transport mechanism becomes more complicated. So far no literature is available to explain the three-phase turbulence modulation or two-phase turbulence with evaporations. Based on the nozzle diameter and jet velocity, the spray jet flow has a typical Reynolds number of 30,000, which means the turbulent effect should be accounted for in this phase-mixing process. In this study, a simple Prandtl Mixing-Length Model (PMLM) is used, in which the effective fluid viscosity is modified by the characteristic turbulence length scale.

3.2.3 Equations of Droplet Trajectory and Evaporation

Velocities and trajectories of droplets are calculated based on Lagrangian trajectory approach, which are given by,

$$m_d \frac{d\vec{v}_d}{dt} = \frac{1}{2} C_d |\vec{v}_{gd}| \vec{v}_{gd} \pi r_d^2 + \frac{1}{2} C_d |\vec{v}_{sd}| \vec{v}_{sd} \pi r_s^2 + m_d \vec{g} \tag{3.7}$$

$$\frac{d\vec{x}_d}{dt} = \vec{v}_d \tag{3.8}$$

Droplet evaporation rate is calculated by (Aggarwal *et al*, 1984)

$$\dot{m} = -4\pi\rho D r_d \ln\left(\frac{y_v(r_\infty) - 1}{y_v(r_d) - 1}\right) \tag{3.9}$$

$$y_v(r_d) = \frac{W_v}{W_v + W_m [p/(p_v(T_d) - 1]} \tag{3.10}$$

3.2.4 Solid-Droplets Interactions

Collision among evaporating droplets and particles is a very complicated phenomenon. No reliable heat and mass transfer model is available, especially for cases with large temperature difference. It is assumed in the present model that particles penetrate or trapped in the colliding droplets upon collision and heat is transferred from a solid particle to the colliding droplet through a vapor film layer around the particle.

3.3 Experimental System for Aspect Ratio Experiment

To investigate the effect of evaporating liquid spray jets in gas-solid flows, an experimental system is set up to produce a continuous gas-solid flow across a long chamber as shown in the Figure 3.1 [25]. This experimental setup includes a

Circulating Fluidized Bed (CFB), a Laser Doppler Velocimetry (LDV), a pressure-controlled evaporating spray jet device, a computerized mass flow rate measurement device, a 48-thermocouple matrix system with a computerized data acquisition, a computerized pressure measurement system, and a laser-enhanced flow visualization and image analysis system.

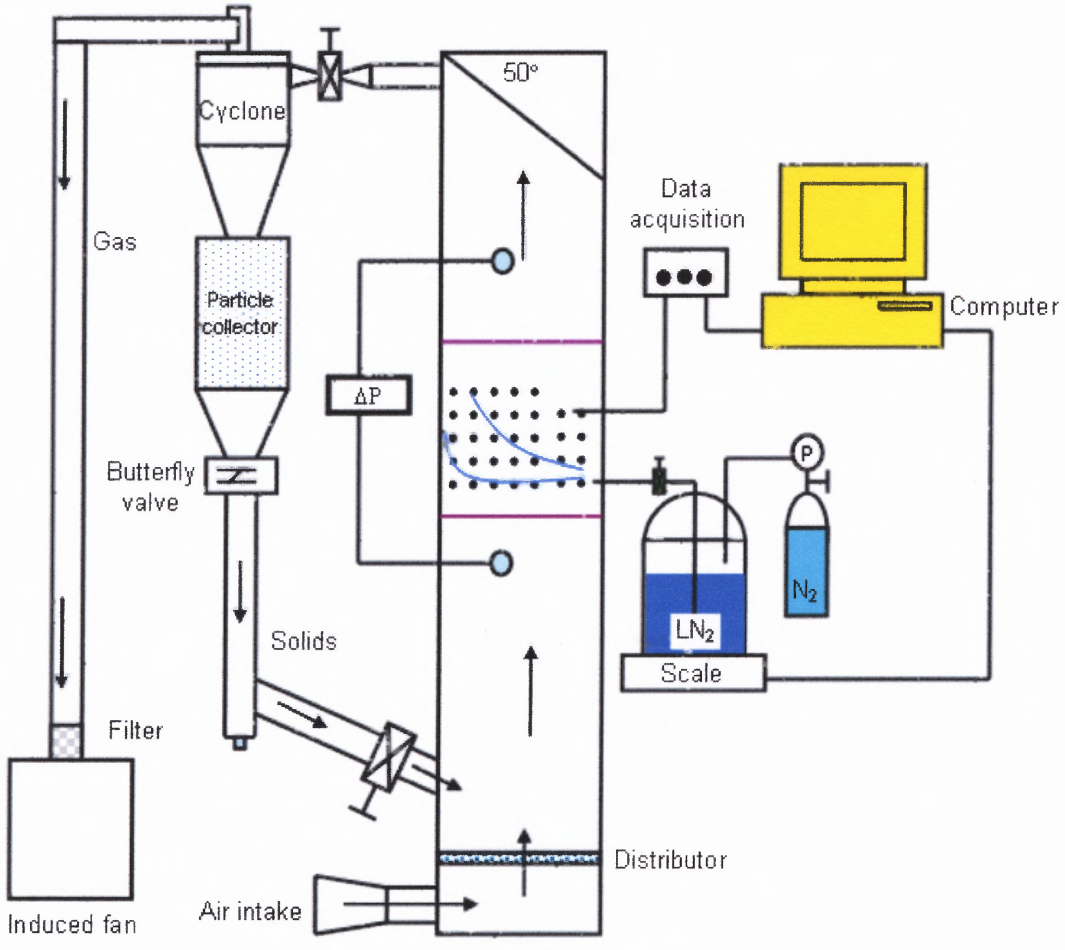

Figure 3.1 Schematic diagram of the experimental system.

The electrostatic charging in the fluidized bed is prevented by carefully grounding the whole setup as well as an anti-static agent was pre-mixed with the FCC powders. Spray jets of liquid Nitrogen produce extremely low temperature inside the

test section which may leads to the cracking of the glass walls. In order to prevent this, both side walls of the test section are reinforced as shown in Figure 3.2. Thermocouple side wall is reinforced by a copper metal plate which also serves as ground medium for any charged particles. A double layer of the glass wall with an air gap in between, to serve as insulation medium, is used on the other side.

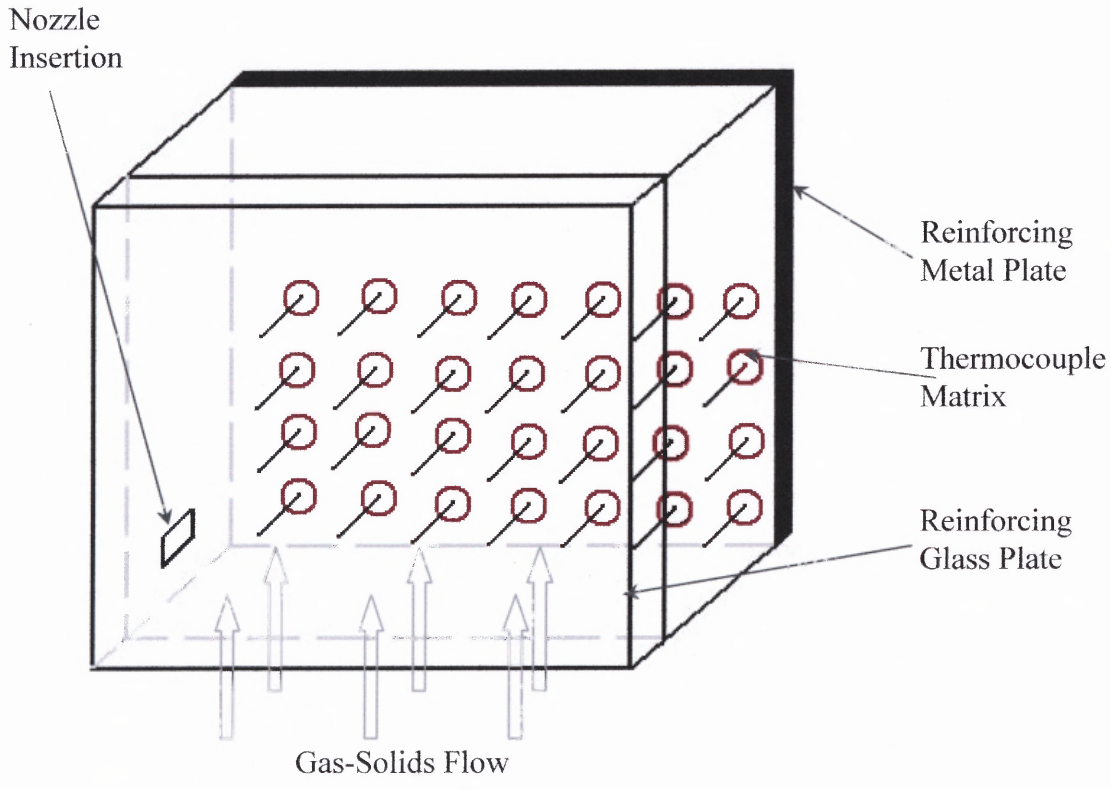

Figure 3.2 Reinforced test section.

A nozzle configuration of b:a = 4:1 means that the ratio of side 'b' to side 'a' is 4 to 1 with a nozzle opening area of 4. Similarly b:a = 1:1 means that the that the ratio of side 'b' to side 'a' is 1 to 1 with a nozzle opening area of 4.

3.4 Experimental Conditions

A flat rectangular nozzle with aspect ratio of 3.8 is used to perform experimental study in both horizontal and vertical orientation. The nozzle hydraulic diameter is calculated to be 1.62 (mm) whereas the spray flow rate ranges 0.9 (lb/min). Spray penetrations in suspensions solid volume fraction of 1.0 is investigated. The spray jet velocity is 28 (m/s). The CFB is operated at the room temperature. The solid particles used in the fluidized bed are FCC particles with a bulk density of 1480 kg/m^3 and the average particle size of 70 μm. The spray liquid is liquid nitrogen.

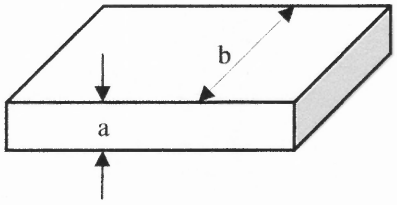

Figure 3.3 Orientation of nozzle

3.5 Problem Statement and Computational Domain

In this study, a cross flow liquid nitrogen spray injected into a steady state, fully developed air-FCC flow have been simulated in a circulating fluidized bed with a rectangular cross-section. Rectangular nozzle is used to provide a liquid nitrogen spray of mean droplet diameter of 160 μm with an injection velocity of 35 m/s and a mass flow rate of 2 g/sec. The horizontal orientation of the nozzle is shown in the Figure 3.3. The nozzle height is denoted by parameter '*a*' and nozzle width is denoted by parameter '*b*'. The air-FCC flow in CFB is at 300 K and 2 m/s. The computational

domain is selected to be 25cm x 2.8cm x 6.75cm with a variable grid distribution of 30 × 20 x 20. In order to investigate the effect of different aspect ratios of rectangular nozzle, 5 nozzles of different aspect ratios but with same exit openness area are used in the numerical study as given in Table 3.1. Nozzle exit fan angle of 5° is used throughout in the entire study. To investigate the effect of solids loading, solids concentration is varied from 0.1 % to 15 %, by volume.

Table 3.1 Nozzle configuration and dimensions for various cases

Nozzle	b (mm)	a (mm)	Exit Area (mm^2)
N-41	4	1	4
N-21	2.8	1.4	4
N-11	2	2	4
N-12	1.4	2.8	4
N-14	1	4	4

3.6 Results and Discussion

3.6.1 Comparison of Experimental and Numerical Results

Experimental and numerical results of spray penetration and spray deflections are compared for rectangular nozzle with aspect ratio of 4:1 in Figure 3.4. The spray jet trajectory is traced by following the lowest temperature on the thermocouple matrix. However, thermocouples above the jet trajectory also show a very low temperature which is due to the evaporation of the droplets and producing the cooling vapors which are carried downstream by the cross flow of gas-solids. Jet trajectory is not very clear at the end of the spray jet as the jet momentum is not very much conserved

rather a mixing zone of the droplet vapors and gas is caused. The comparison shows that the numerical prediction is well in accordance with the experimental results. The penetration length seems to be slightly under predicted by simulation results. A jet penetration length is determined by the droplet size distribution along the jet trajectory where 75 % of the initial jet mass is evaporated i.e., the droplet diameter is reduced from 160 μm to 100 μm.

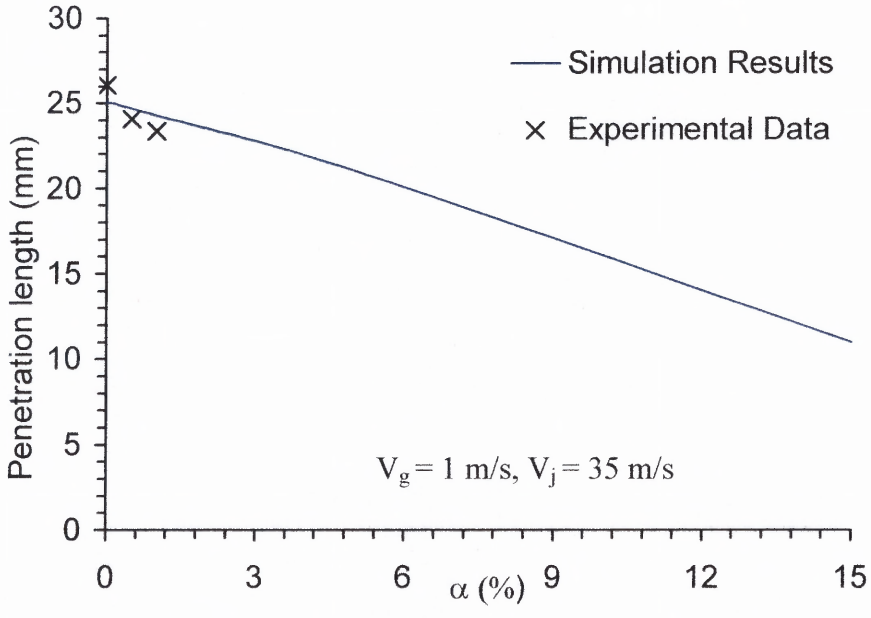

Figure 3.4 Experiment and simulation results comparison of horizontal orientation of N41.

3.6.2 Effect of Aspect Ratio on Evaporation Length and Spray Deflection

Effect of aspect ratio on spray evaporation length is shown in Figure 3.5 for a solid volume fraction of 15 %, which shows that the spray evaporation length is not significantly altered by the change in aspect ratio. The jet is penetrated inside the simulated section almost completely at 90° to the cross-flow. At the end of the spray

jet, as the droplets inside the jets become smaller owing to a strong evaporation effect, the jet deflection is achieved.

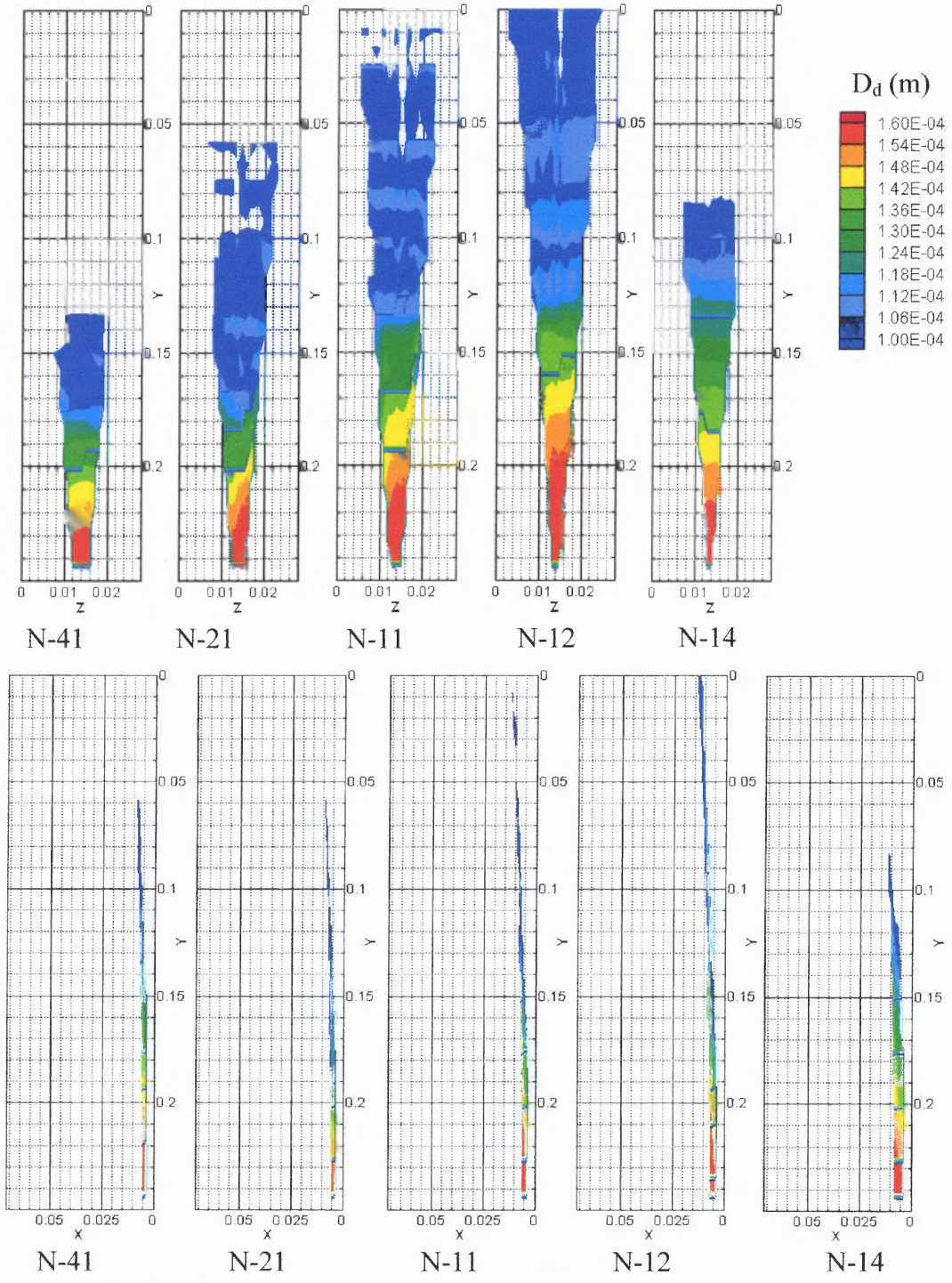

Figure 3.5 Effect of aspect ratio with α = 15 %.

As the aspect ratio of nozzle is changed from 4:1 to 1:1, the penetration length is increased. This is due to the spray jet structure in the initial part of the spray jet. For 4:1 aspect ratio, the longer side of the jet is in direct contact of the gas-solids cross-flow, causing a more rigorous collision between the droplets and solids and hence reducing the penetration length. However, as the jet becomes flat in vertical direction, jet momentum is preserved for a longer time as a reduced area is available for the droplet and gas-solids interaction. This causes the jet to penetrate longer inside the jet. For a limiting case of 1:4 aspect ratio, the penetration length is decreased, however this length is still 25% longer than that of a 4:1 nozzle. For this case, larger sides of the spray jet (parallel to gas-solids flow) tend to expand under the influence of nozzle exit fan angle. Due to this expansion, a large amount of the liquid is expanded causing the jet momentum to be reduced. As the momentum is reduced, the jet penetration is reduced.

3.6.3 Effect of Solids Loading on Evaporation Length

Figure 3.6 shows the effect of increasing solids loading on the spray jet structure from a 4:1 aspect ratio nozzle. Solids loading are increased from 0.1 % to 15 %. For a lower solids loading, i.e., 0.1 % and 1 %, there is no significant difference in the spray pattern, however as the solids loading is further increased, penetration length is reduced. For a 5% solids loading, the length is reduced by 20 % where as penetration length is almost reduced to half when solids loading is increased to 15 %. This result is in accordance with previous findings that the penetration length is a strong function of solids loading [19].

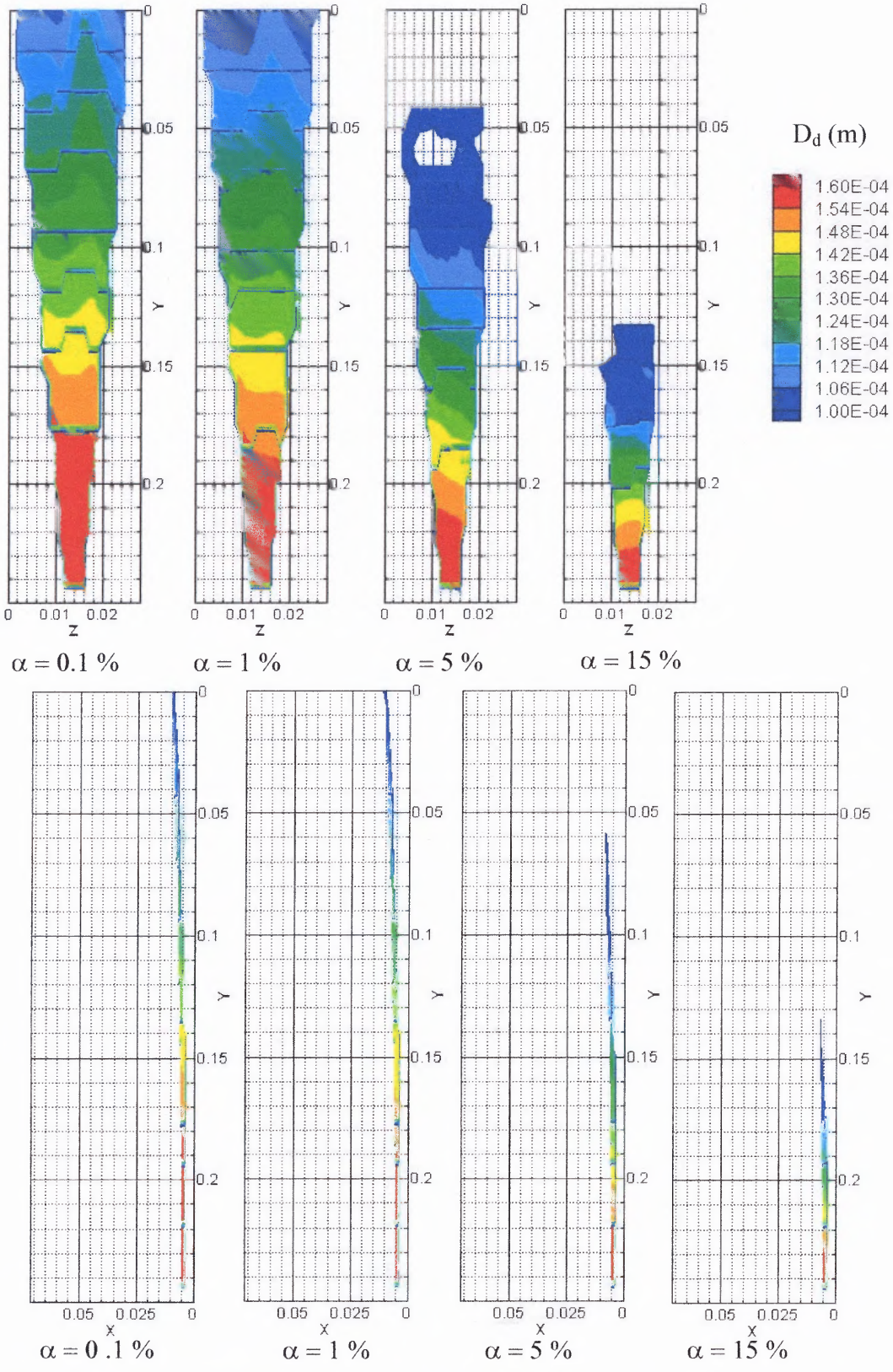

Figure 3.6 Horizontal configuration of 4:1 aspect ratio nozzle.

3.6.4 Effect on Solids Loading Along and Around the Jet

Figure 3.7 shows the distribution of solids concentration at the central plane of the nozzle along the gas-solids flow inside the flow structure for different aspect ratios. Rapid evaporation of liquid spray in a gas-solid flow results in an excessive vapor production that dilutes the local solid concentration. It can be seen that the dilution effect of solids produces a region that is deviated away by convection from the main spray under the influence of cross-flow. It is noted that vapor expansion leads to a compression effect producing a condense layer of solids that is further compressed between the vapor region and the main spray jet region. This compressed layer can be clearly seen just above the spray entrance near the central plane. The vapor expansion also slightly increases the solid concentration in the main stream in the riser.

Figure 3.8 shows the solids concentration at a cross-sectional plane at the nozzle exit. It is interesting to find a dense layer of solids surrounding the diluted region (as explained above). This surrounding layer is more significant for a horizontal flat nozzle rather for a vertical flat nozzle. This is due to the fact that a horizontal flat nozzle causes a relatively uniform collision between solids and droplets which in turn causes a larger dilution region. As the dilution region is large, it compresses the solids more and hence a thicker surrounding region with higher the solids concentration is achieved.

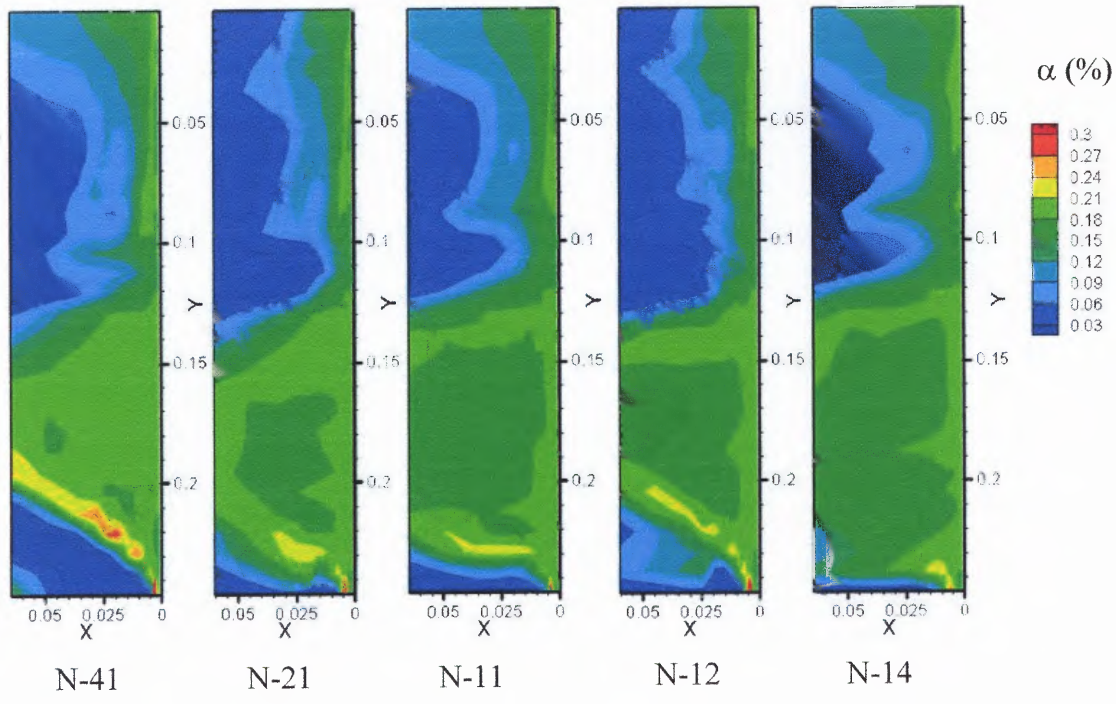

Figure 3.7 Solids concentration at the central plane.

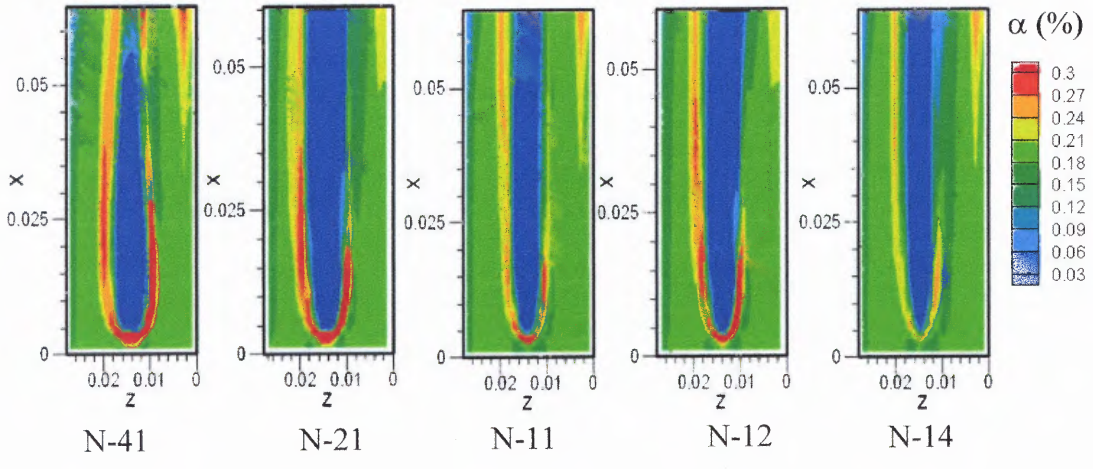

Figure 3.8 Solids concentration at the nozzle exit plane.

3.6.5 Effect on Spray Width and Spray Height

Figure 3.9 shows the change in spray width 'b' and spray height 'a' along the spray penetration. This change is under the influence of the nozzle fan angle. However, as the fan angle is same for all the cases, the change in the spray width also follows the same line. Spray height exhibit almost no change during the initial part of the spray jet. However, once the jet is expanded enough to be influenced by the cross flow, spray height starts to decrease.

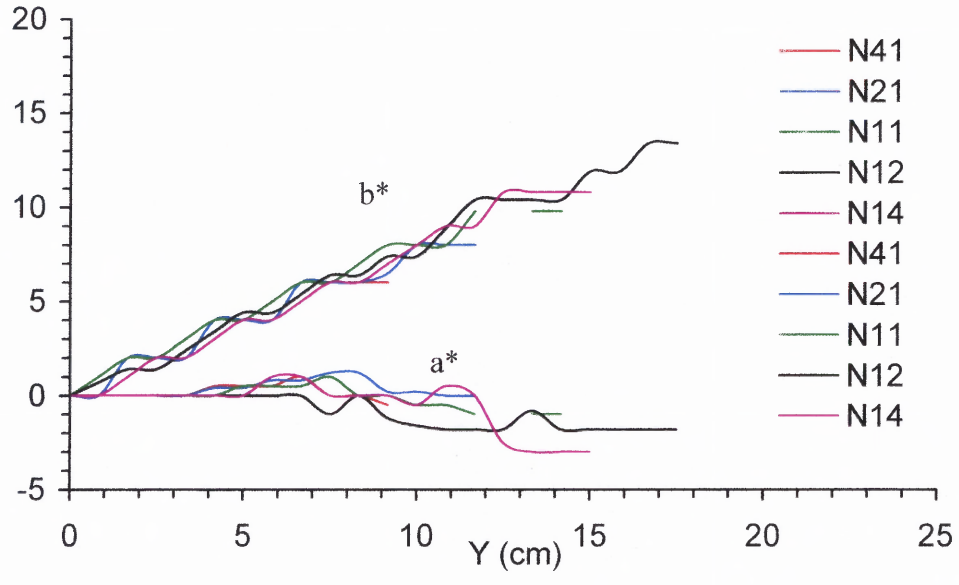

Figure 3.9 Change in spray width and spray height along the jet trajectory.

3.7 Conclusions

The effect of the aspect ratio of rectangular nozzle is studied in regards to the penetration length and spray deflection. A 3-D numerical simulation code is developed to study the parametric effect of nozzle aspect ratio on the phase interaction and the spray structures in gas-solids suspensions. Spray structures

produced from the rectangular nozzle are different from the circular nozzles. In addition, decreasing aspect ratios of the rectangular nozzles cause the penetration length to increase for a constant solid volume fraction. The effect of increasing solid volume fraction causes the penetration length to decrease. Spray deflection is found to be a function of the droplet size. As the droplet size decrease due to evaporation along the jet trajectory, the spray deflection becomes more significant. Due to the cross-flow of the gas-solid medium through spray region, vapors are deviated away from the jet trajectory which causes the dilution in the solids concentration above the nozzle region. This dilution region is surrounded by a dense layer of solids which is more significant for horizontal nozzle than vertical nozzle.

3.8 Future Study

3.8.1 Detailed Flow Structure

It will be interesting to see a very detailed flow structure of the spray for various aspect ratios. A closer look at the flow structure can indicate more influencing parameters of the flow such as the evaporation rate distribution, vapor deflection pattern, gas velocity distributions and solids entrainment inside the spray jet.

3.8.2 Concurrent Rectangular Spray Jet

It is more convenient to simulate various aspect ratios of spray under concurrent gas-solid flow. This study will reveal whether the velocity, temperature and concentration similarities holds true for rectangular spray jets or not. This information is necessary for simplification of the modeling work.

CHAPTER 4

EFFECT OF FAN ANGLE OF RECTANGULAR NOZZLE ON FLOW STRUCTURE

4.1 Problem Statement and Computational Domain

In this study, a cross flow liquid nitrogen spray injected into a steady state, fully developed air-FCC flow has been simulated in a circulating fluidized bed with a rectangular cross-section. The computational domain is selected to be 15cm x 8cm x 7.15cm with a grid distribution of 30 × 20 x 20, as shown in Figure 4.1 (a). A rectangular nozzle of 1×4 mm is used to provide a liquid nitrogen spray of mean droplet diameter of 160 μm with an injection velocity of 35 m/s and a mass flow rate of 2 g/sec. The horizontal orientation of the nozzle is shown in the Figure 4.1 (b). The nozzle height is denoted by parameter '*a*' and nozzle width is denoted by parameter '*b*'. The air-FCC flow in CFB is at 300 K and 2 m/s. In order to investigate the effect of nozzle exit fan angle on spray evaporation, two sets of numerical simulations are compared, one with 5° fan angle and the other with 30° fan angle. A solid concentration of 15 %, by volume, is used throughout the entire study.

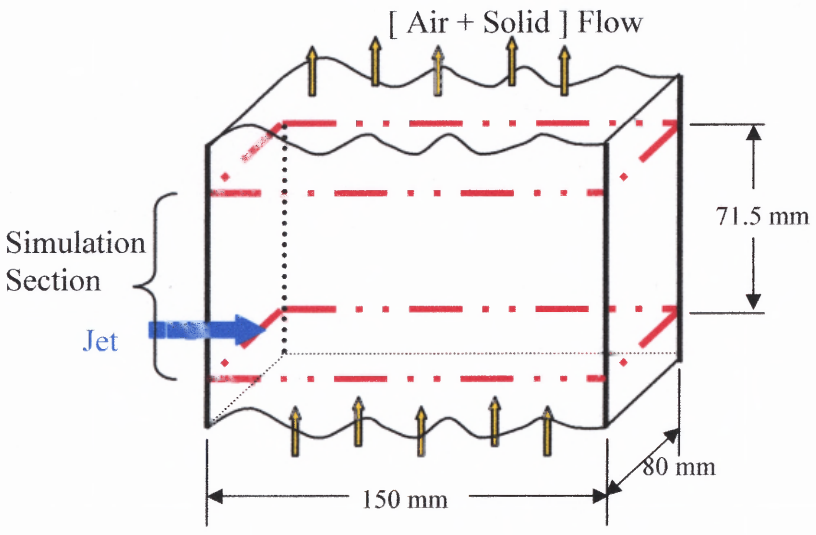

(a) Domain geometry

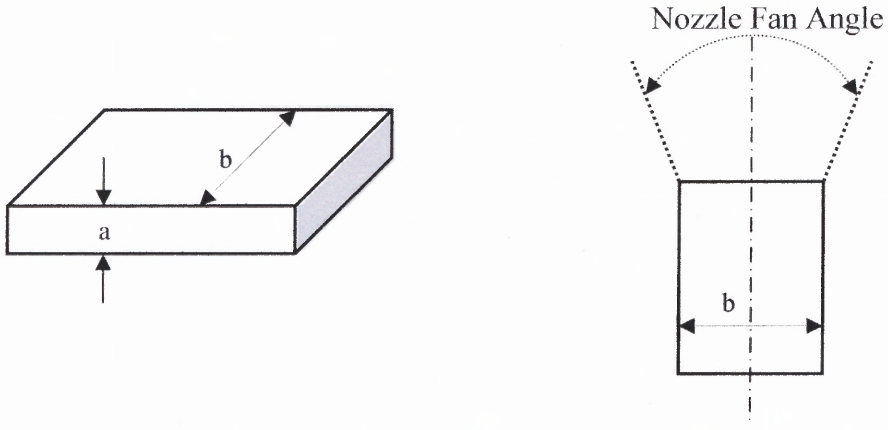

(b) Configuration of horizontal rectangular nozzle and illustration of fan angle

Figure 4.1 Computational domain geometry and nozzle configuration.

4.2 Results and Discussion

4.2.1 Effect of Fan Angle on Evaporation Length and Spray Deflection

Effect of fan angle on spray evaporation length is shown in Figure 4.2, which shows that the spray evaporation length is not significantly altered by the fan angle. In a previous study, it has been validated that the spray penetration is a strong function of the solids loading rather any other parameter [19]. The penetration length is greatly reduced in the presence of a very dilute solid concentration when compared with no solid concentration; however this effect becomes insensitive with the increase in solids loading at higher solid concentrations. In this study a high solid concentration of 15 %, by volume, is used in both cases. Hence, a comparable penetration length in both cases validates that the spray evaporation length is a weak function of the fan angle. Similar to the penetration length, the spray jet deflection shows little difference with the change in fan angle.

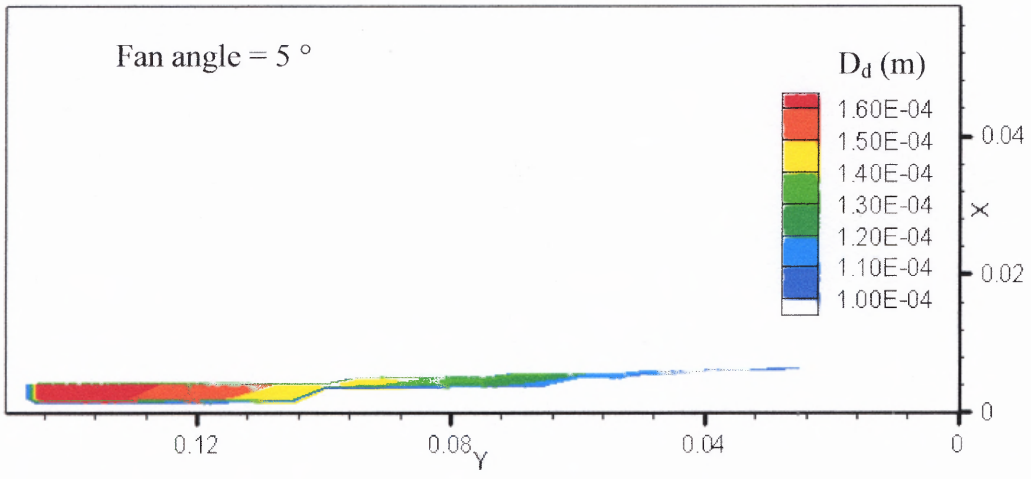

(a) Spray with 5° fan angle

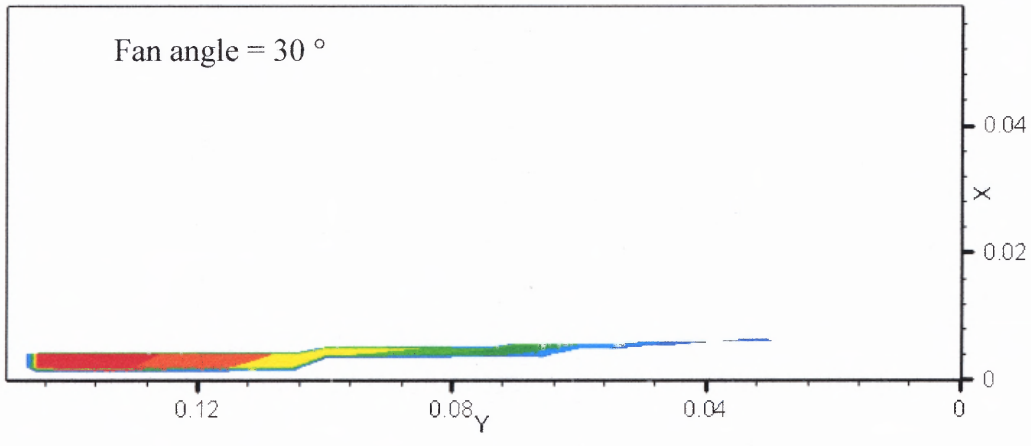

(b) Spray with 30° fan angle

Figure 4.2 Side view of spray evaporation and deflection at the center plane.

4.2.2 Effect of Fan Angle on Spray Expansion

A significant change can be noticed in the spray expansion as shown in Figure 4.3. The jet with 30 ° fan angle is expanded much more as compared to the spray jet with 5° fan angle. A wider spray jet ensures that a large area of gas-solid flow is influenced and the spray droplets contact with the solids more uniformly than that with a narrower jet.

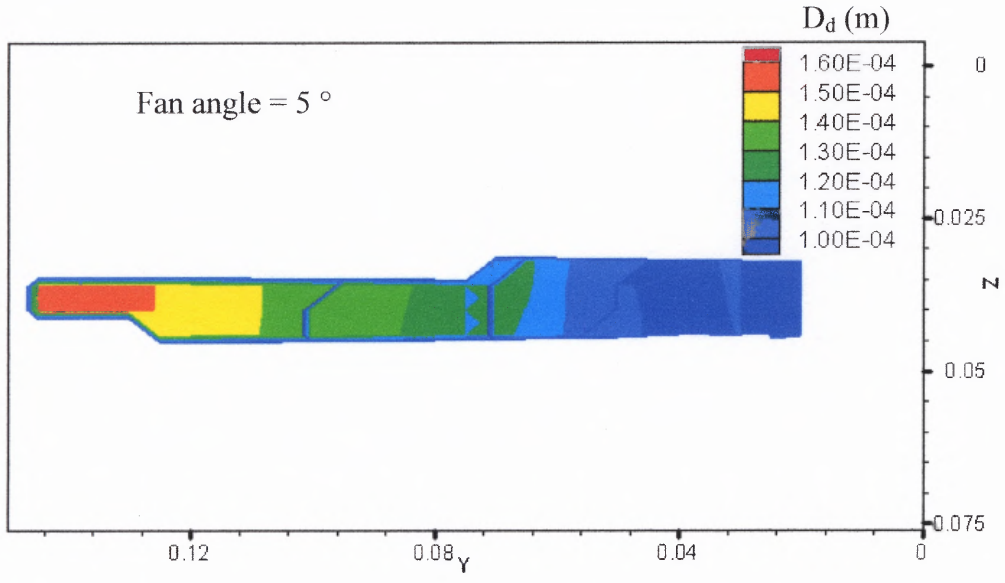

(a) Spray with 5° fan angle

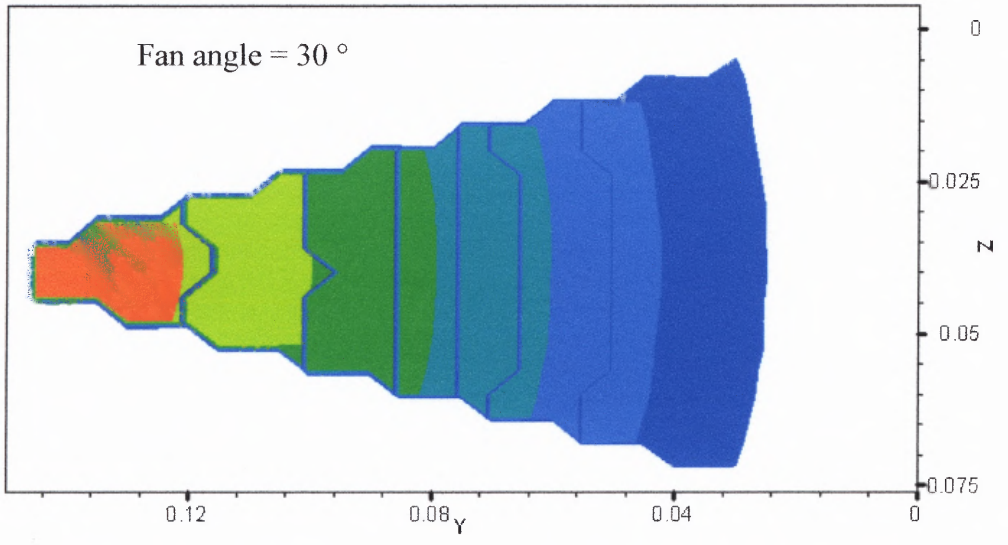

(b) Spray with 30° fan angle

Figure 4.3 Top view of spray expansion and coverage.

4.2.3 Effect of Evaporation on Gas Temperature Distribution

Rapid evaporation of droplets in a gas-solid flow also leads to a reduction in temperature of the gas and solids due to the absorption of latent heat from the surrounding gas-solid media. The contours of gas temperature at the central plane of the jets are shown in Figure 4.4. As the spray droplets are penetrating into the cross-flow of gas-solid media, the gas cools downs as it passes across the spray jet. Due to the higher evaporation rates of the droplets in the initial part of their trajectory, the gas temperature distributions deviates from the spray trajectory in the initial part of the jet as well. Droplets keep going straight very much along the original injection direction but the evaporated vapor quickly engulfed into the wake region formed by gas-solid convection over the spray trajectory. This result is due to the cross flow convection effect of gas-solid medium.

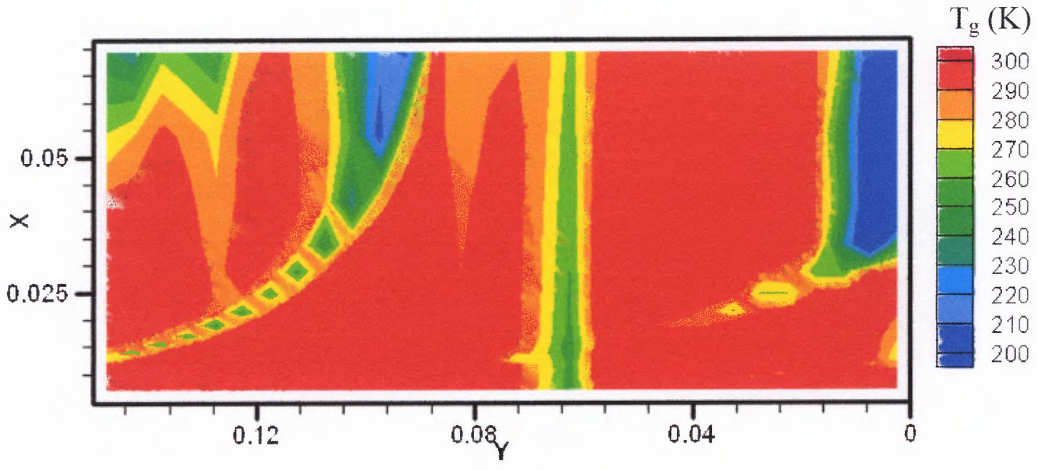

(a) Fan angle 5°

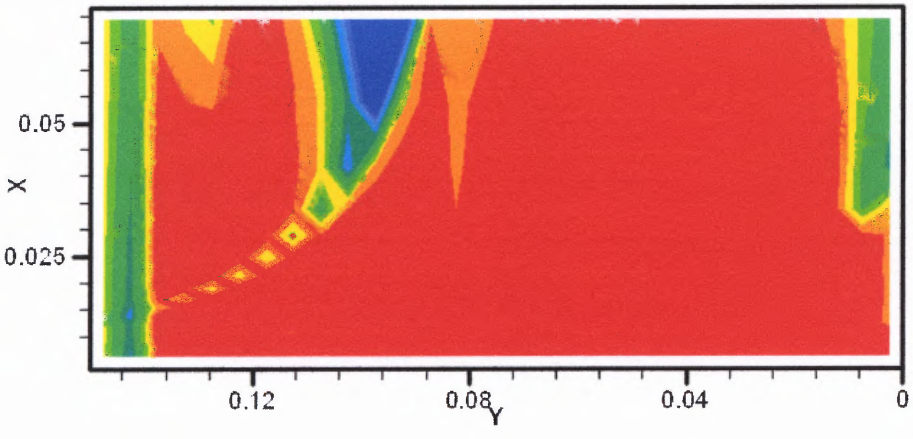

(b) Fan angle 30°

Figure 4.4 Gas temperature distributions in the central plane.

The effect of fan angle, however, can be seen along the two side walls. For a smaller fan angle where the droplets are confined in the narrow area, the gas immediately downstream to the nozzle has no severe effect of vapor convection. For spray with a wider fan angle, droplets come in contact with more solids and evaporate quickly, the gas medium above the nozzle cools down due to convection. Conversely,

at the end of penetration, more liquid droplets from the spray with a smaller fan angle are impacting on the opposite wall surface, leading to a noticeable gas temperature reduction at the center plane as shown in Figure 4.4(a).

4.2.4 Effect of Evaporation on the Dilution of the Solid Concentration

The rapid evaporation of liquid spray in a gas-solid flow results in an excessive vapor production that dilutes the local solid concentration. Figure 4.5 shows a three-dimensional distribution (layer-by-layer effect) of solid concentration inside the riser for the case of 30° fan angle. It illustrates the dilution effect of solids in a region that is deviated away by convection from the main spray under the influence of cross-flow. It is noted that vapor expansion leads to a compression effect producing a condense layer of solids that is further compressed between the vapor region and the main spray jet region. This compressed layer can be clearly seen just above the spray entrance near the central plane. The vapor expansion also slightly increases the solid concentration in the main stream in the riser.

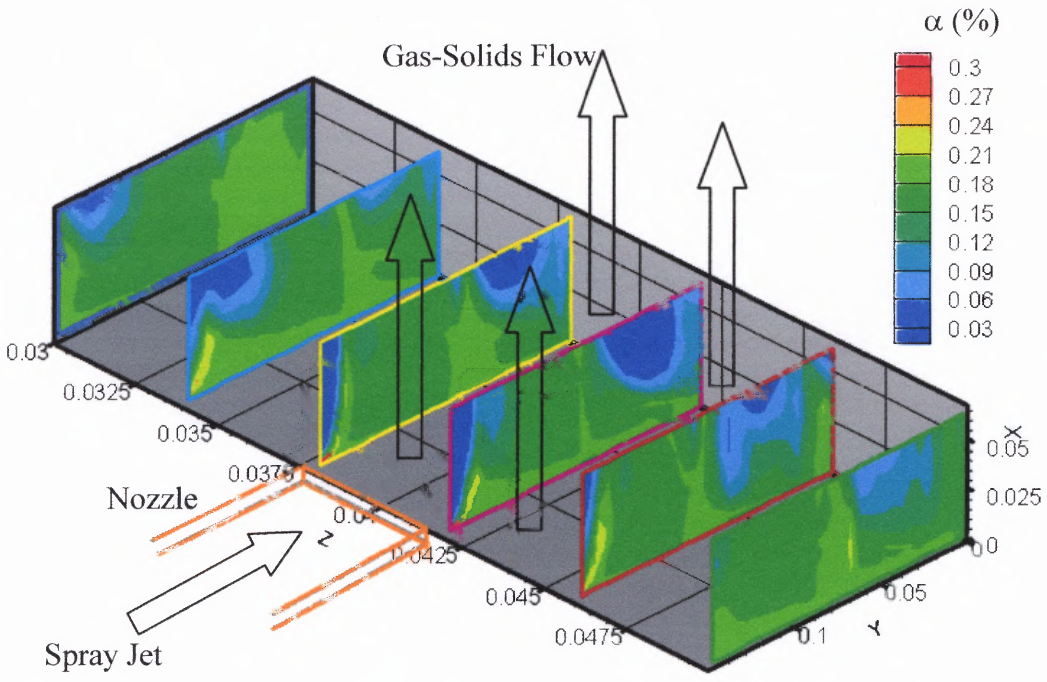

Figure 4.5 Solid concentration distribution (with spray fan angle of 30°).

4.2.5 Comparison of Evaporation Rate

Figure 4.6 shows the distribution of the total evaporated mass in the area covered by the spray for both cases. It can be seen from the figure that both evaporation rate curves have the same structure with an initial peak which indicates that a high percentage of evaporation occurs during the initial part of the jet. It is also clear that for bigger fan angle nozzle, the total evaporation is higher than the nozzle with smaller fan angle. This is due to the reason that a wider expansion of the spray causes the interaction with more solids, thus causing more droplets to evaporate.

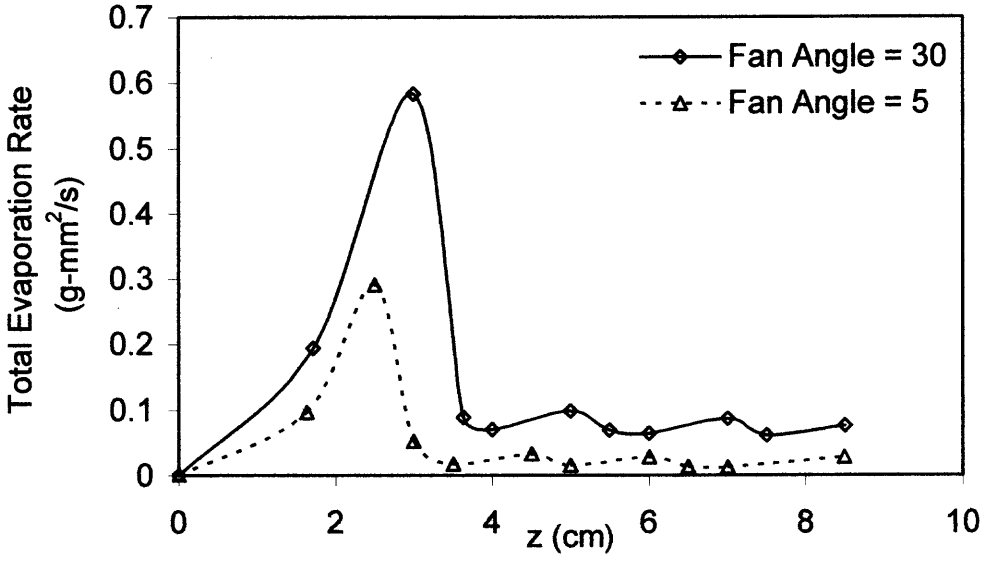

Figure 4.6 Distribution of mass evaporated per unit area along the jet trajectory.

4.3 Conclusions

Three dimensional numerical simulations have been performed for the cross-flow liquid nitrogen sprays into an air-FCC rectangular CFB riser. Similar configuration of the nozzle, with two different fan angles (5° and 30°) was used to investigate the effect of nozzle fan angle on spray structure. Due to higher solid loading, a little

change in both spray evaporation length and spray deflection can be seen for both cases. Due to the strong cross-flow convection, the temperature contours of gas and solids phases are significantly deviated from the spray trajectory. With spray evaporation, the solid concentration in the vapor region is diluted from 15% to 3% while a dense layer of solids surrounding the vapor region. The temperature depletion up to 50 K is obtained in solids phase. The cross-section of the spray after exiting from the rectangular nozzle maintains a basic rectangular shape but with varied aspect ratios and sizes along the spray penetration path. However the shape of the vapor cross-section is no longer rectangular due to the flow convection and vapor evaporation.

CHAPTER 5

PHASE TRANSPORT IN A TYPE II LEIDENFROST COLLISION

5.1 Introduction

Droplet-solid collisions in the Leidenfrost regime have many practical applications, such as spray quenching of metal alloys or firewall [26, 27], spray quenching of melting debris from explosion, and chemical spray into hot solids [18]. In FCC applications, the FCC particles are pre-heated to a very high temperature before the liquid crude oil is sprayed on a dense gas-solids medium. The interaction mechanism between the solid particle and the liquid droplets is Leidenfrost collision mechanism. The true physical mechanism is very complex due to complex phase interactions between the gas, solids and liquid. This interaction mechanism, however, is the fundamental key for the flow characteristic of spray in gas-solids suspension. A rapid evaporative interaction may lead to a less penetration length as well as less deflection. On the other hand, a slow evaporation may cause the agglomeration of the solid particle and eventually collapse the suspended gas-solids bed. So, it is very important to quantify the parameters governing the interaction mechanism.

5.1.1 Type I Leidenfrost Collision

In the experimental aspect, many researchers presented a sequence of photographs showing the deformation process of liquid droplets impacting on a hot flat surface. An experimental study is carried out to investigate the deformation process of a saturated water droplet of about 2 mm in diameter impacting on a polished gold surface heated to 400°C [27]. They suggested that the impact and breakup of water

droplets could be grouped into three general categories depending upon the droplet Weber number. Using different liquids such as water, ethanol and acetic acid, [28] performed photographic studies to determine the deformation behavior of droplets impacting a horizontal copper surface heated up to 400°C. Their results support the classifications proposed by [27]. However, it is difficult to identify the critical Weber number, which is scattering in the range of 50 to 90 [29, 30]. Recently Hatta *et al.* investigated the collision dynamics on a hot rough surface and found that the surface roughness leads to the asymmetric and irregularity droplet deformation [31]. The experiments of Bernardin *et al.* [32] found that the temperature corresponding to the critical heat flux and the Leidenfrost point showed little sensitivity to both droplet velocity and impact frequency. For droplets oblique impinging on a solid surface, an investigation of the loss of momentum of the droplets, the droplet deformation, and the onset of droplet disintegration in an oblique collision process is carried out [33]. A minimum impinging angle is found for droplet disintegration. Below this impinging angle no droplet disintegration is observed.

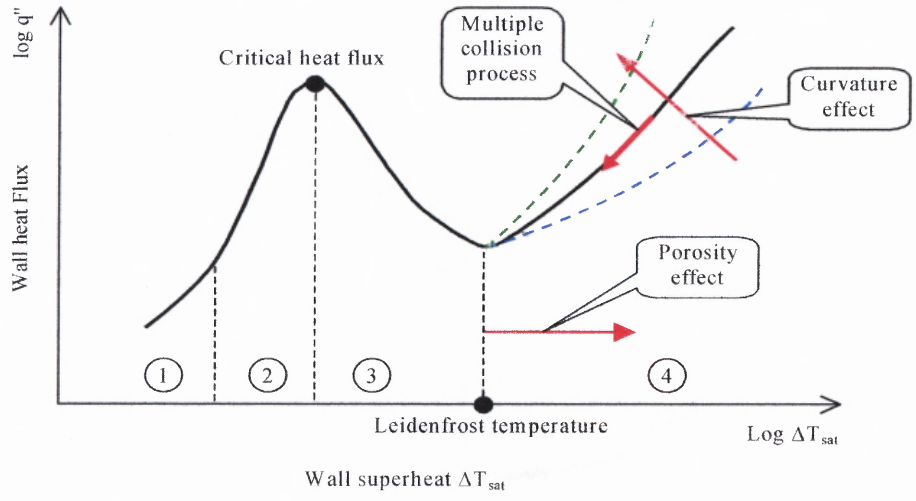

Figure 5.1 Evaporation regimes.

The time dependence of droplet-particle contact surface area during the collision process is crucial to modeling the droplet hydrodynamic and heat transfer behaviors. First order period of a freely oscillating droplet is used to describe the contact time [27], however, the second power of contact time is found to be proportional to the contact radius [34]. A correlation for the droplet contact time in the Leidenfrost regime was proposed [28]. It is found that, at a low collision velocity, the droplet spreads out into a thin film before boiling and the deformation area had a linear relation with the contact time [35]. A dilute mist flow over a hot body is modeled by assuming the collisions are the same as a droplet with a planar surface [36]. Their prediction, however, is yet to be validated by experiments.

5.1.2 Type II Leidenfrost Collision

In FCC application, the solid particles are preheated to elevated temperature before a spray is injected into the riser. The reactor temperature is approximately 800 °C to 900 °C while the liquid droplets temperature is around 200 °C. Here the collision mechanism is truly Leidenfrost, however, the collision mechanism is supposed to be different than the type I Leidenfrost collision, as the particle has limited heat capacity unlike the unlimited heat capacity of solid surface in type I. In addition, the droplet surface behavior may significantly affect the dynamic behavior of vapors generated. Hence, the collision of super heated solid particles with liquid droplets is called Type II Leidenfrost collision. Despite a number of reported studies on droplets impinging on a large flat solid surface with an infinitely large heat capacity, limited research has been reported on the effects of solid surface curvature or limited heat capacity of solids for the Leidenfrost collisions.

5.1.3 Objectives of Modeling

In the conclusions of the previous two chapters, it is evident that the most dominant liquid solid interaction occurs in the initial part of the spray. From application point of view, the liquid droplets size is as large as 400 μm in FCC applications where as the size of FCC particles is 70 μm. Hence, the collision mechanism is actually between a large liquid droplet and a small solid particle. The droplet evaporates due to strong heat transfer during this collision. It is important to note that as the droplet size reduces to 70 μm (comparable to the FCC particle size), 99% of the liquid volume is evaporated already. This proves that the heat transfer is purely dominant by the Type II Leidenfrost collision mechanism. This study focuses on the development of initial understanding for type II Leidenfrost collision mechanism. Firstly, this phenomenon is captured visually with the help of experimental setup. Several sets of experiments show different modes of collision mechanism. Mechanistic models are developed to study the parametric effects on heat transfer during these modes of type II Leidenfrost collision.

5.2 Experimental System for Type II Leidenfrost Collision

The experimental setup was developed to generate mono-sized solid particles at a very high temperature. The micro-arc generation system uses an electrical circuit to produce a high voltage drop across the metallic wire and neighboring cathode which produces an electric arc in between. The metal temperature increases and when it reaches the melting point of the wire material the wire melts. Finally a drop of the liquid metal is formed at the tip of the wire. This drop of molten metal falls down due

to its weight and due to the electrical push. A water reservoir is used at the bottom to collect the particles. A high speed (500 fps) digital camera is used to capture the sequence of images during the collision of the droplet to the water surface. Superimposed images of the particle result in a series of solid particle positions in a single image. By calibrating the time between the two positions, the velocity of the particle is calculated along its trajectory. An optical pyrometer is used to draw the temperature profile of the solid particle along its trajectory.

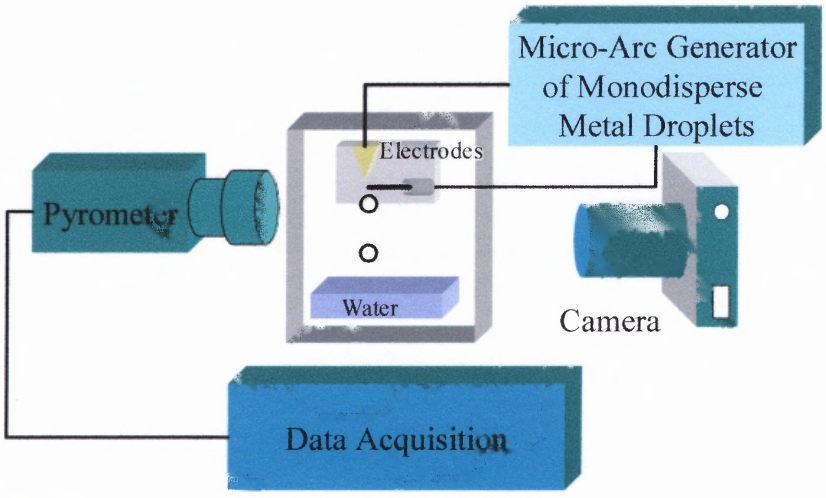

Figure 5.2 Schematic diagram experimental setup for type II Leidenfrost collision.

Several types of experiments are conducted using the above apparatus. First the particle is allowed to cool only in the air as shown in figure 5.3. Then, a water pool is placed below to collect the hot particles. Three types of modes were detected when a molten copper particle hit the water surface. The three modes are shown in the Figure 5.4.

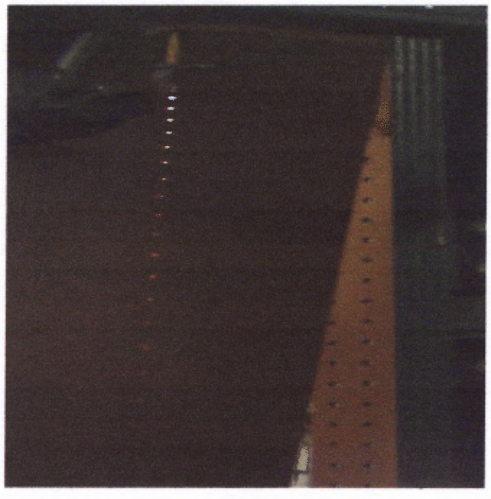

Figure 5.3 Particle cooling in air.

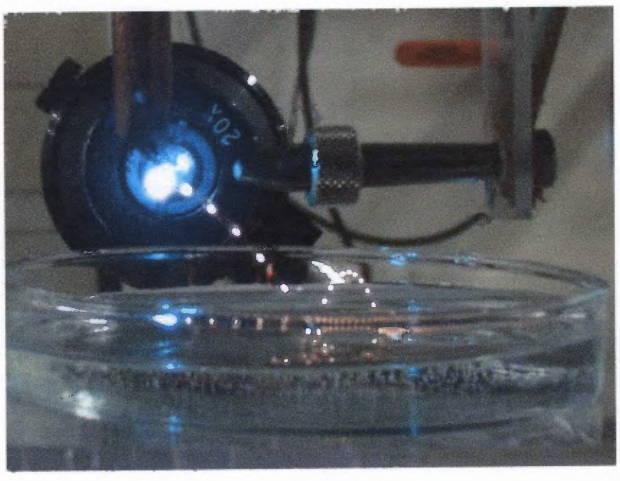

(a) Molten copper particle bouncing off the water surface.

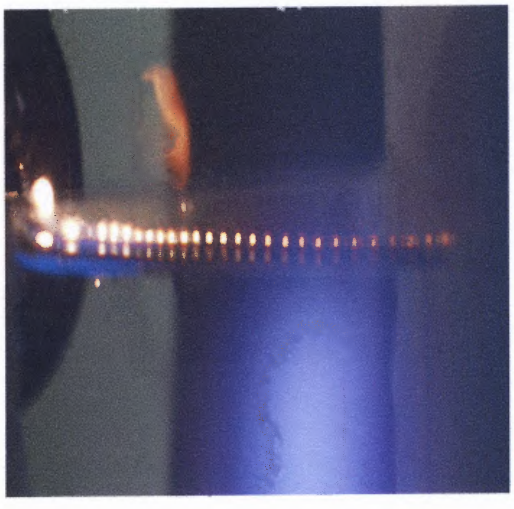

(b) Molten copper particle hitting water surface and traveling on the water surface.

(c) Molten copper particle shooting through the water and cooling.

Figure 5.4 Experimental observations of type II Leidenfrost collision.

5.3 Normal Collision Mechanistic Model of Type II Leidenfrost Collision

Consider a small hot solid particle moving with a velocity U_p. The temperature of the particle is T_p. Assuming Rp/Rd <<1, this process can be simulated with a small hot particle colliding with a large flat liquid surface.

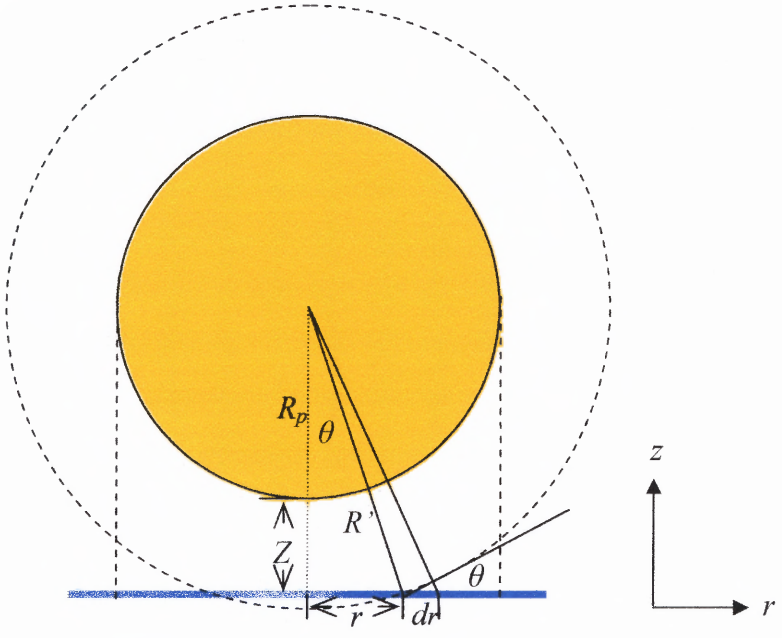

Figure 5.5 Heat transfer due to radiation.

$$R' = \sqrt{r^2 + (R_p + z)^2} \tag{5.1}$$

At any location 'r' on the liquid surface, heat transfer between the infinitesimal particle surface and infinitesimal the liquid surface due to radiation is given by

$$dQ_r = (\varepsilon_p \sigma T_p^{\,4}) A_p dF_{pl} - (\varepsilon_l \sigma T_l^{\,4}) dA_l F_{lp} \tag{5.2}$$

$$A_p dF_{pl} = dA_l F_{lp} \tag{5.3}$$

$$dQ_r = [(\varepsilon_p \sigma T_p^{\ 4}) - (\varepsilon_l \sigma T_l^4)] A_p dF_{pl} \tag{5.4}$$

$$dF_{pl} = \frac{dA_p}{4\pi R'^2} \tag{5.5}$$

$$dA_p = 2\pi r dr \cos\theta \tag{5.6}$$

$$\cos\theta = \frac{R_p + Z}{\sqrt{(R_p + Z)^2 + r^2}} \tag{5.7}$$

$$dQ_r(r) = 2\pi r dr \frac{(R_p + Z)R_p^2}{[(R_p + Z)^2 + r^2]^{3/2}} \sigma(\varepsilon_p T_p^4 - \varepsilon_l T_l^4) \tag{5.8}$$

Radiation heat transfer per unit area,

$$q_r = \frac{dQ_r(r)}{2\pi r dr} \tag{5.9}$$

$$q_r = \frac{(R_p + Z)R_p^2}{[(R_p + Z)^2 + r^2]^{3/2}} \times \sigma(\varepsilon_p T_p^4 - \varepsilon_l T_l^4) \tag{5.10}$$

Heat due the conduction,

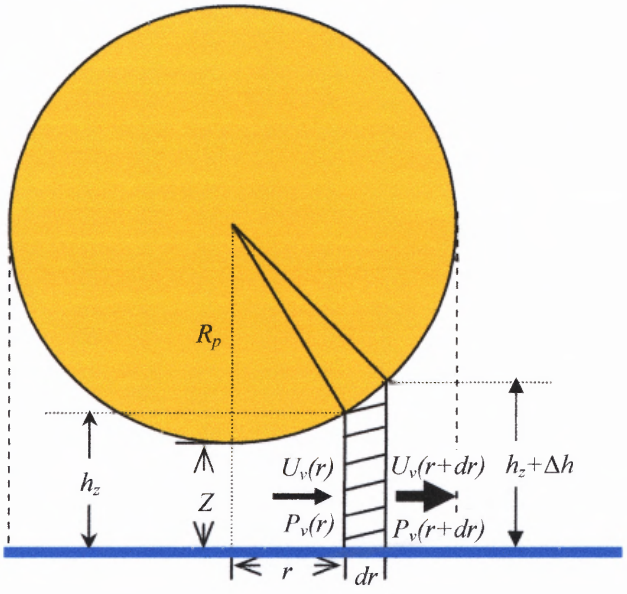

Figure 5.6 Heat transfer due to conduction.

Consider a circular region of thickness 'dr' at radius r from the center of the water surface. The heat transfer to this area due to conduction only is given by the following

$$dQ_c = 2\pi r\, dr\, k_c \frac{T_p - T_l}{(R_p + z) - \sqrt{R_p^{\,2} - r^2}} \tag{5.11}$$

Heat transfer per unit area is given by

$$q_c = \frac{dQ_c}{2\pi r dr} \tag{5.12}$$

$$q_c = k_c \frac{T_p - T_l}{(R_p + z) - \sqrt{R_p^{\,2} - r^2}} \tag{5.13}$$

The total heat per unit area is calculated by adding the heat due to conduction and heat due to radiation.

$$q_T = q_r + q_c \tag{5.14}$$

This total heat transfer is causing the surface of the water to evaporate.

$$q_T = \dot{m}_v L \tag{5.15}$$

where $\dot{m}_v$ is the mass of vapors generated per unit area and L is the latent heat of vaporization.

According to the mass balance of the control volume,

$$\begin{aligned} &\rho_g 2\pi r dr h_z(t) + \rho_g 2\pi r h_z U_v(r,t)dt + \dot{m}_v 2\pi r dr dt \\ &-\rho_g 2\pi(r+dr)(h_z + \Delta h)U_v(r+dr,t)dt = \rho_g 2\pi r dr h_z(t+dt) \end{aligned} \tag{5.16}$$

$$\rho_g\left[\frac{h_z(t+dt)-h_z(t)}{dt}\right] - \rho_g h_z(t)\left[\frac{U_v(r+dr,t)-U_v(r,t)}{dr}\right] + \dot{m}_v = \rho_g U_v(r+dr,t)\left[\frac{h_z}{r} + \frac{\Delta h}{dr}\right] \tag{5.17}$$

By definition,

$$\frac{[U_v(r+dr,t)-U_v(r,t)]}{dr}=\frac{\partial U_v}{\partial r}$$
$$\frac{h(t+dt)-h(t)}{dt}=-U_p \tag{5.18}$$

Substitution the Equation 5.18 in Equation 5.17,

$$\dot{m}_v+\rho_g U_p-\rho_g h\frac{\partial U_v}{\partial r}=\rho_g U_v(r,t)[\frac{h_z}{r}+\frac{\Delta h}{dr}] \tag{5.19}$$

where

$$\Delta h=dr\frac{r}{\sqrt{R_p^{\,2}-r^2}} \tag{5.20}$$

The Equation 5.19 provides the distribution of vapor velocity along the 'r' direction.

Applying the momentum balance to the vapor volume in r direction only,

$$P_v(r)2\pi r h_z dt-P_v(r+dr)2\pi(r+dr)(h_z+\Delta h)dt$$
$$=\rho_v[U_v^{\,2}(r+dr)2\pi(r+dr)(h_z+\Delta h)dt-\rho_v U_v^{\,2}(r)2\pi r h_z dt \tag{5.21}$$

$$\frac{P_v(r)-P_v(r+dr)}{dr}-[P_v(r+dr)+\rho_v U_v^{\,2}(r+dr)][\frac{\Delta h}{h_z dr}+\frac{1}{r}]=\rho_v\frac{U_v^{\,2}(r+dr)-U_v^{\,2}(r)}{dr} \tag{5.22}$$

$$\frac{P_v(r)-P_v(r+dr)}{dr}=-\frac{\partial P}{\partial r}$$
$$\frac{U_v^{\,2}(r+dr)-U_v^{\,2}(r)}{dr}\approx 2\rho_v U_v\frac{\partial U_v}{\partial r} \tag{5.23}$$

$$-\frac{\partial P_v}{\partial r}-[P_v(r)+\rho_v U_v^{\,2}(r)][\frac{\Delta h}{h_z dr}+\frac{1}{r}]=2\rho_v U_v\frac{\partial U_v}{\partial r} \tag{5.24}$$

The equation (5.24) provides the vapor pressure distribution under the particle. This pressure causes the force to balance the weight of the particle as the particle comes down. The pressure force is given by the following expresion

$$F_p = \int_0^{R_p} (P(r,t) - P_a) 2\pi r dr \tag{5.25}$$

The velocity of the particle is calculated by the following expression

$$m\frac{dU_p}{dt} = -F_p - F_D \tag{5.26}$$

where F_D is the drag force on the particle and can be calculated as

$$F_D = 3\pi\mu U_p d \tag{5.27}$$

Now the force of vapors generated is not only balancing the weight of the particle but also providing the force to repel the particle.

Considering the lumped body model for the particle heat transfer,

$$mC\frac{dT_p}{dt} + \sum Q_i = 0 \tag{5.28}$$

$$Q_i = Q_r + Q_c \tag{5.29}$$

where Q_r is the total heat transfer due to radiation from the particle. This includes the heat radiated to the liquid surface as calculated by Equation 5.10, as well as $Q_{r\,(to\ room)}$ which is the radiation heat transfer to the room. Q_c is the total heat lost by the particle due to convection. This includes the heat conduction Q_{cond} to the liquid surface as calculated by the Equation 5.13 and the other part is the heat transfer due to convection Q_{cs} to the surrounding air, where Qcs is calculated by the following expression.

$$Q_{cs} = h_c A(T_p - T_\infty) \tag{5.30}$$

where h_c is the convective heat transfer coefficient and is given by

$$h_c = \frac{N_u k}{d_c} \tag{5.31}$$

where Nusselt number, N_u for an immersed sphere is given by the following equation.

$$N_u = 2 + 0.6 \mathrm{Re}^{0.5} \mathrm{Pr}^{1/3} \tag{5.32}$$

Using the above model, the particle temperature and velocity is solved for a molten copper particle falling on a water surface. The complete collision time and heat transfer are simulated. The initial temperature of the particle is 3000 K and the water surface is assumed to be on saturated temperature of 373K, so that all the heat provided to water is consumed in the phase change i.e., vapor generation. The effect of gravity is neglected for simplicity. The effect of buoyancy and basset force are also neglected. Other parameters used in this case study are summarized in the table 5.1.

Table 5.1 Material properties and initial conditions for the case study

	Water	Copper Particle	FCC Particle
Temperature (K)	373	3000	1200
Emissivity	0.1	0.1	0.1
Latent heat of vaporization (J/Kg)	2260000	-	-
Radius (m)	-	400e-6	70e-6
Density (kg/m^3)	-	8900	1480

5.4 Results and Discussion

5.4.1 Experimental Validation

Figure 5.7 shows the comparison of the model prediction with the experimental results of [37]. In the experiments, a molten copper particle is allowed to cool in an Argon only environment. The argon environment is used to minimize the effect of chemical reaction i.e., oxidation on the particle surface. More details about the experimental conditions and setup can be found in [37]. The temperature profiles were noted using pyrometer system at two different locations while the particles were falling down. The model simulated the same experimental conditions and the temperature of the particle is calculated along its trajectory. The model prediction matches very well with the experimental data that partially validate the Leidenfrost model presented in this study.

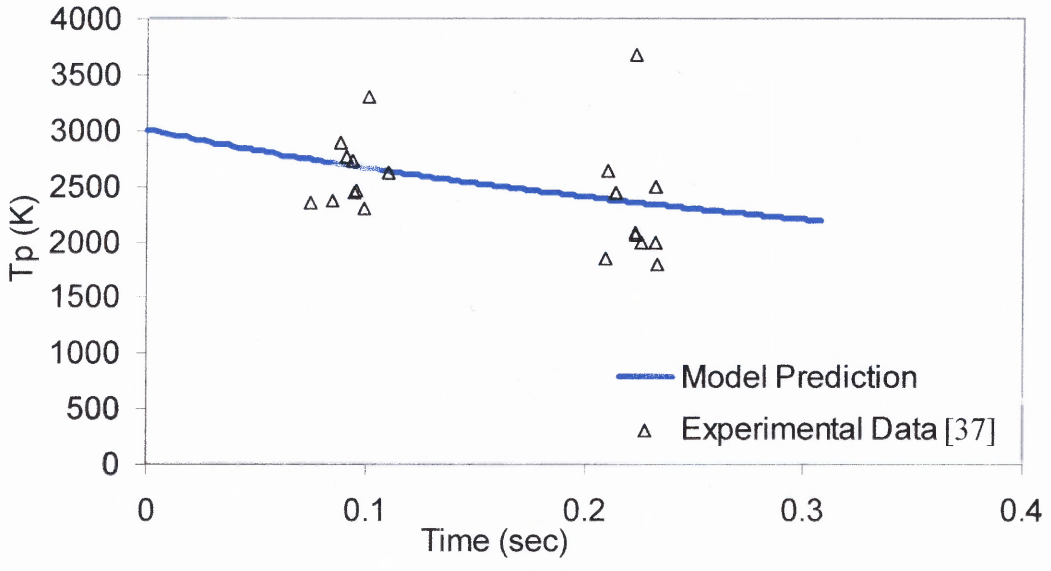

Figure 5.7 Temperature variation of the particle cooling in the Argon only environment.

5.4.2 Leidenfrost Collision

Figure 5.8 shows the temperature profile of a molten copper particle falling over a water surface. The particle initial temperature is 3000K with an initial downward velocity of 1.5 m/s. The initial gap between the particle and the water surface is 0.1m. This initial gap is high enough to ensure that the effect of radiation and conduction to the liquid surface is negligible. The particle is push with an initial velocity towards the water surface. During the initial pat of the approach the particle is loosing heat due to radiation and convection to the ambient and the heat loss to the liquid surface is negligible. However, very close to the water surface, the heat loss to the water surface due to radiation and conduction is significant. However, the Leidenfrost collision time is very small in this case. Hence the temperature variation is not very much effected by the collision. Figure 5.9 shows the variation of the temperature of the particle along its trajectory. This figure clearly shows the bouncing off phenomenon of the hot particle. As the particle bounces of the water surface, it is still loosing heat to the liquid and ambient and the temperature of the particle is still falling.

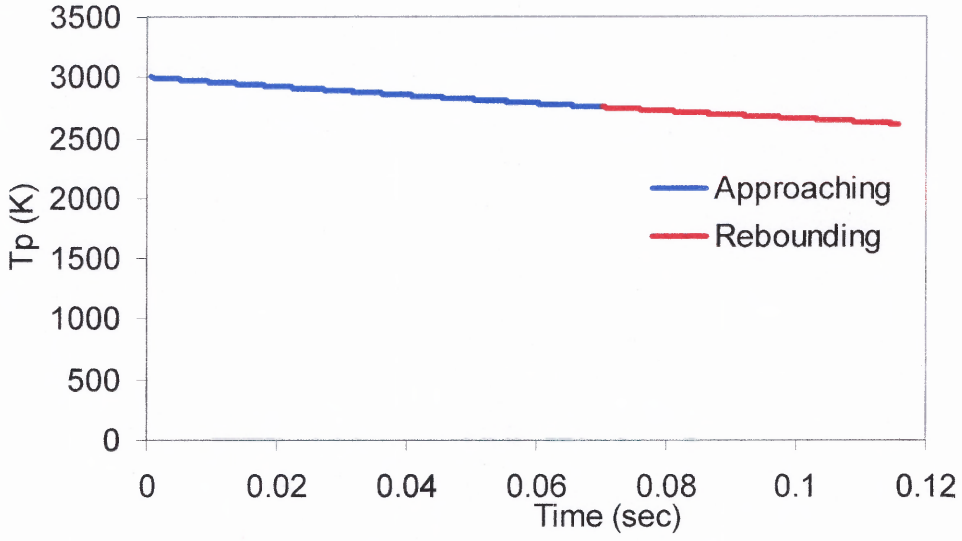

Figure 5.8 Temperature variation of the particle during the Leidenfrost collision with water surface.

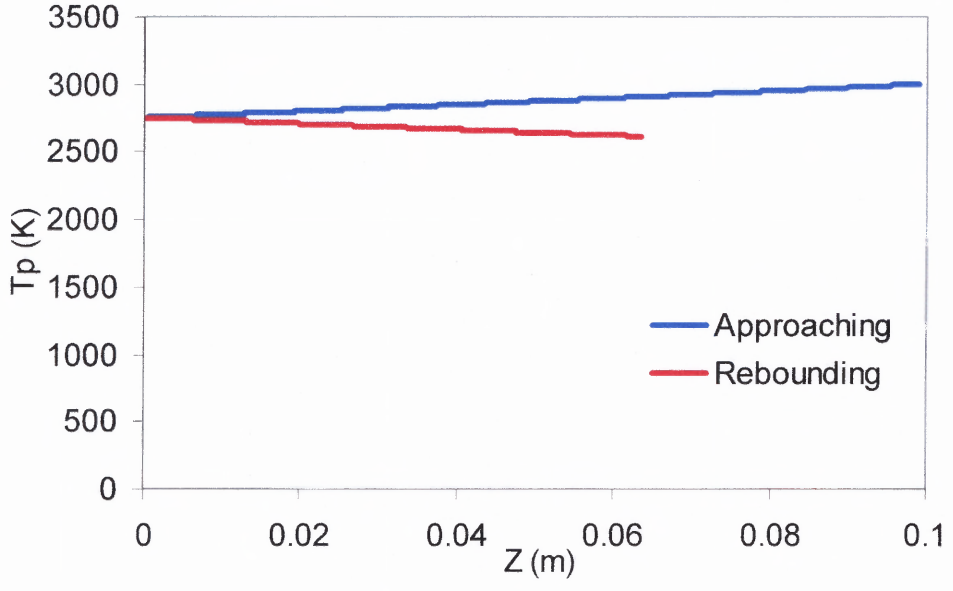

Figure 5.9 Temperature variation of the particle along its trajectory.

Figure 5.10 shows the total heat transfer to the liquid only. It can be seen from this figure that the collision duration is very small for which the heat transfer to the liquid surface is significant. This duration is termed as Leidenfrost duration. In this case the Leidenfrost duration is less than 200 μs. Another important factor to be noted in this figure is the different shape of the two curves. The approach curve increases very rapidly as the particle is close to water surface and the heat transfer goes to maximum. However, during the bouncing off the particle heat loss to the water surface is decreasing as the distance is increasing, however, the vapor present on the top of the water surface is still hot and it is constantly loosing heat to liquid surface. Hence, the heat loss to water surface during the rebounding process takes more time than the approach process.

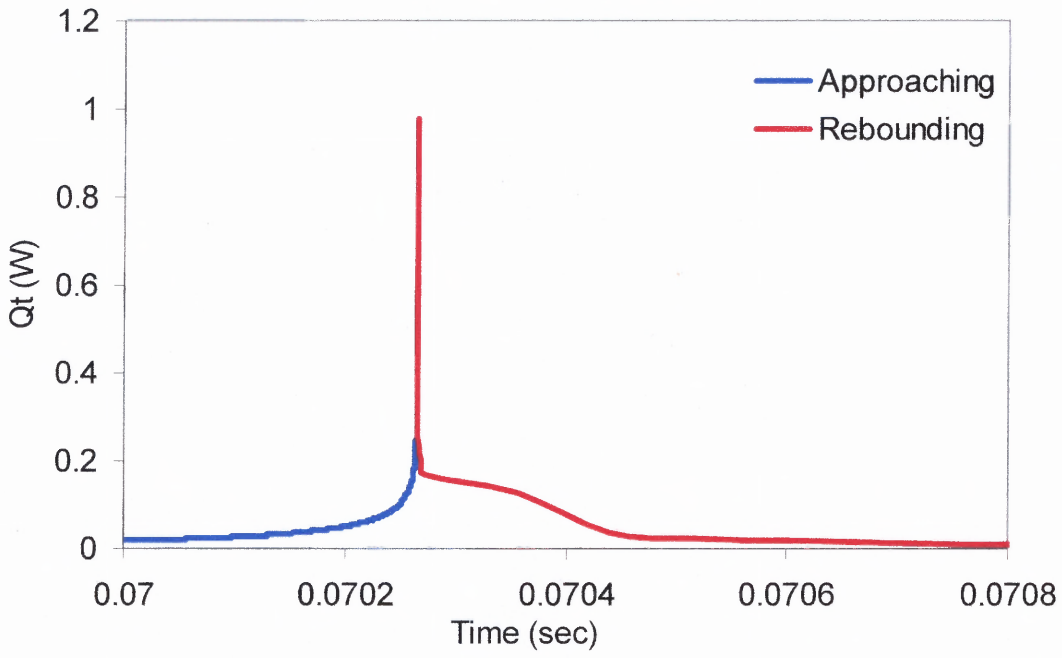

Figure 5.10 Heat transfer to the liquid surface during the collision where particle is closest to the liquid surface.

Figure 5.11 shows the ratio of accumulated mass of vapor generated to the total mass of vapors generated along the trajectory of the particle. When the particle is far away, the ratio is very small which means that the vapors generation is very small and when the particle is close to the water surface, the vapors are generated more easily and rapidly as more energy is available for the vaporization. The maximum vapors are generated when the particle is closest to the water surface. The vapors generated during this process provides a cushioning effect on the particle and a net pressure force is exerted on the particle which first balances the inertia force of the particle and the particle velocity becomes zero. However, the particle temperature is still very high and the vapor generation continues.

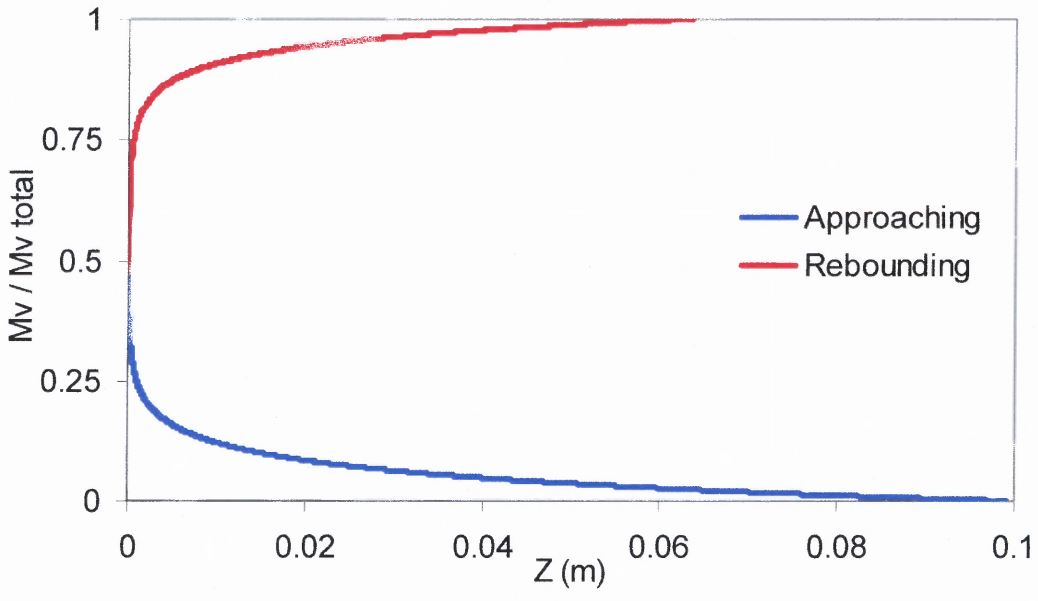

Figure 5.11 Ratio of mass of vapor generated to the total vapors generated during the collision process.

The additional vapors generated provide the excessive pressure force which causes the particle to bounce off the water surface. As the particle bounces off the surface, it still looses the heat to the water surface and the vapors are generated.

However, as the distance between the particle and the liquid surface is increasing, the heat transfer is decreasing and the vapor generation rate is decreasing as shown by the upper red curve of Figure 5.11. In this case the total mass of vapor generated is 3.08E-11 Kg.

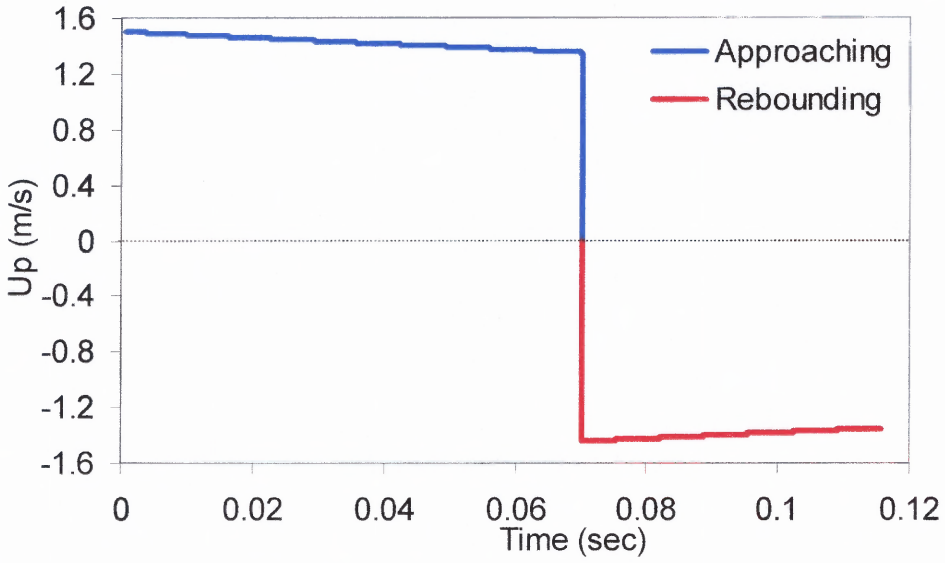

Figure 5.12 Velocity variation of the particle during the collision.

Figure 5.12 shows the variation of the velocity during the complete collision process. In the approaching curve the velocity of the particle is decreasing under the effect of the drag only. When the particle is very close to the water surface the effect of pressure force causes a sudden decrease of the particle velocity and the particle velocity decrease quickly. However, the particle is repelled by the excessive vapors generated. The bouncing off velocity is slightly higher than the approach velocity. This may be due to the reason that during the rebounding process the pressure force is much greater than the drag which causes the particle to accelerate quickly in the initial part of the bouncing off process. In the bounce off process the, the pressure

force is decreasing until it becomes insignificant. At that point the calculations stop. The accumulated mass generated until that moment is called the total mass vapor generated.

5.4.3 Effect of Initial Temperature of the Particle

Figure 5.13 shows the effect of initial particle temperature on the particle temperature during the Leidenfrost collision. In all the following figures, the approach and bouncing off process is shown by single curve.

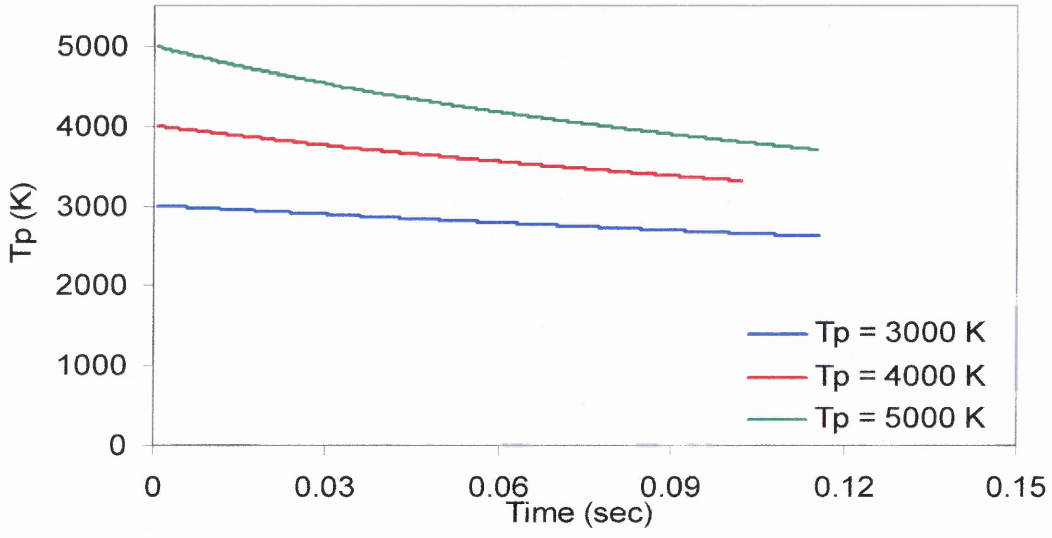

Figure 5.13 Temperature variation of the particle during the complete Leidenfrost collision with different initial temperatures.

Figure 5.14 shows the heat transfer to the liquid during the collision process. It is clear from the figure that as the initial temperature of the particle is higher, the particle temperature close to the water surface is also higher and due to that fact, the particle looses more heat to the water surface. If the particle initial temperature if 5000K the heat lost to water surface during the Leidenfrost collision is more than

1.4W as compared to less than 1W when the initial particle temperature is 3000K. This is about 40 % difference.

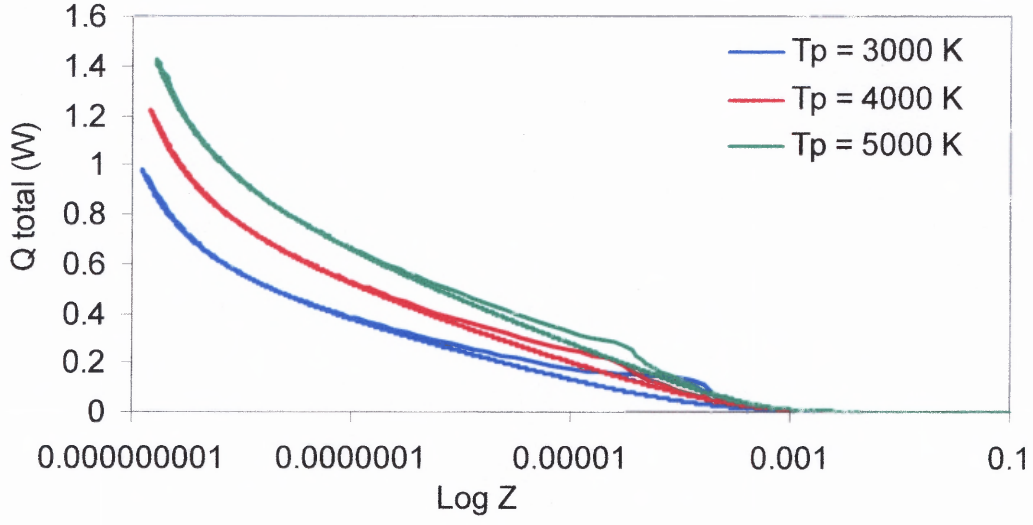

Figure 5.14 Heat transfer to the liquid surface with different temperature particles.

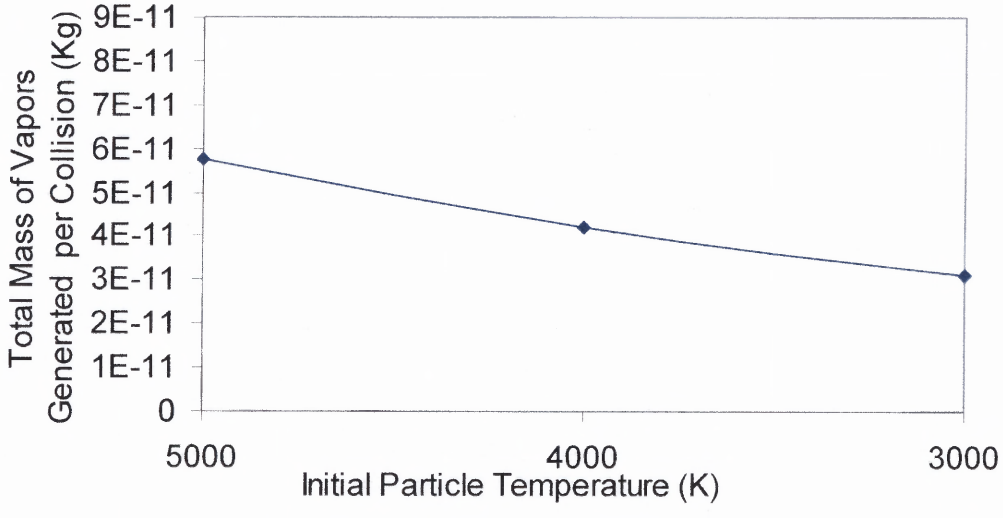

Figure 5.15 Total vapors generated per collision for different initial temperature of particle.

5.4.4 Effect of Initial Velocity of the Particle

In this case, the particle with initial temperature of 3000K is pushed towards the water surface with three different initial velocities i.e., 1.5 m/s , 1.0 m/s and 0.5 m/s. All other parameters are same. Figure 5.16 shows the effect of initial velocity on the particle temperature profile. It shows that as the particle velocity is small, it takes more time to reach the water surface and during which it looses more heat to the surrounding. It is also clearly seen in the figure 5.17 that smaller the particle velocity, the lower its temperature when reached the eater surface.

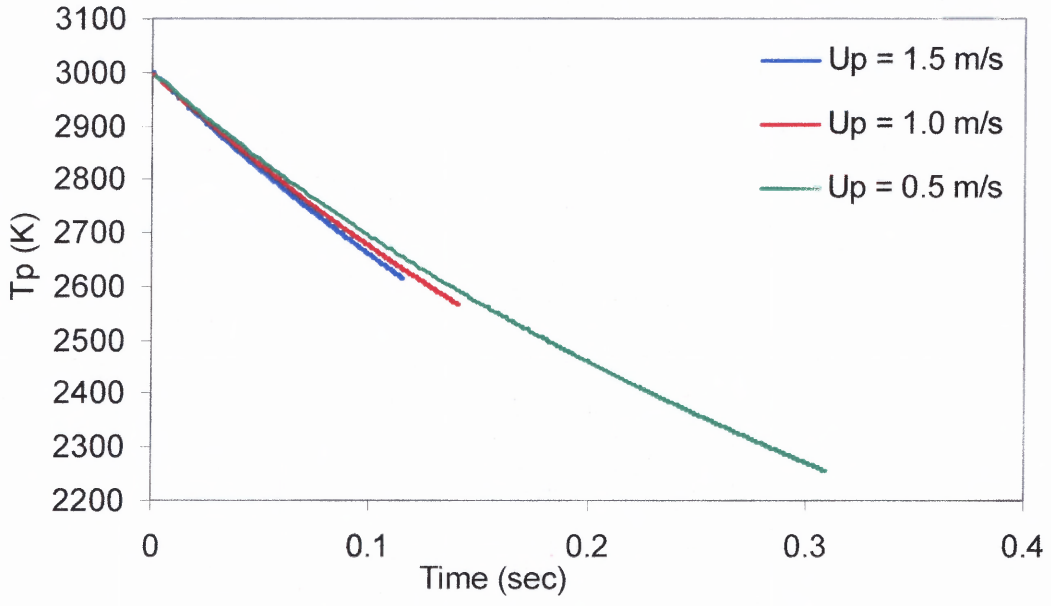

Figure 5.16 Temperature variation of the particle during Leidenfrost collision with different initial velocities.

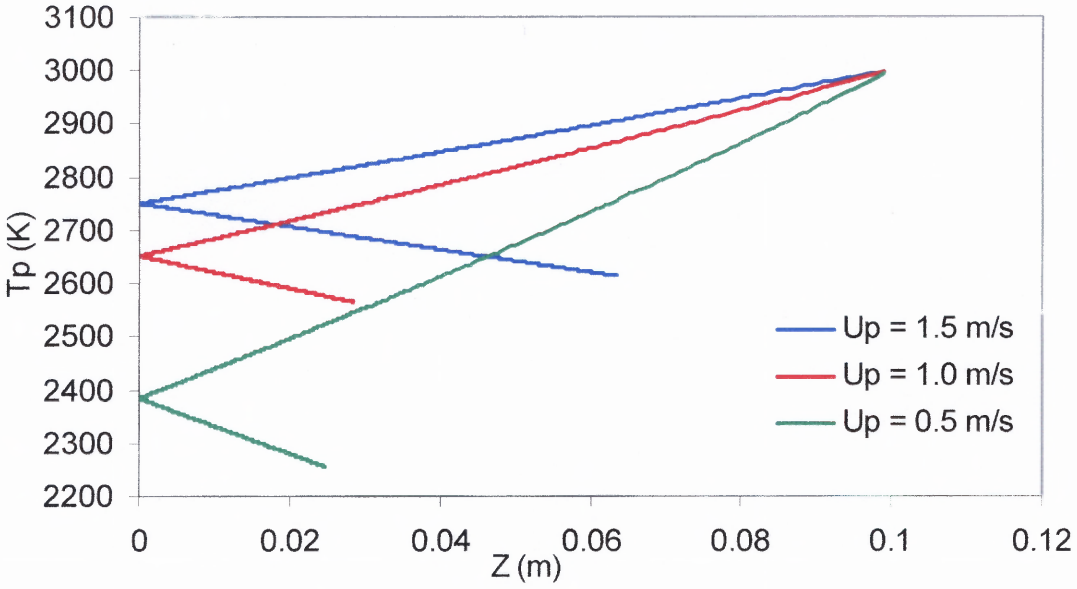

Figure 5.17 Temperature variation of the particle along the trajectory during Leidenfrost collision with different initial velocities.

Figure 5.18 shows the velocity profiles of all three different initial velocity cases. It is clearly evident from the figure that the bouncing off velocity is comparable to the approach velocity, however, as the approach velocity is higher, the bouncing off velocity is higher as well.

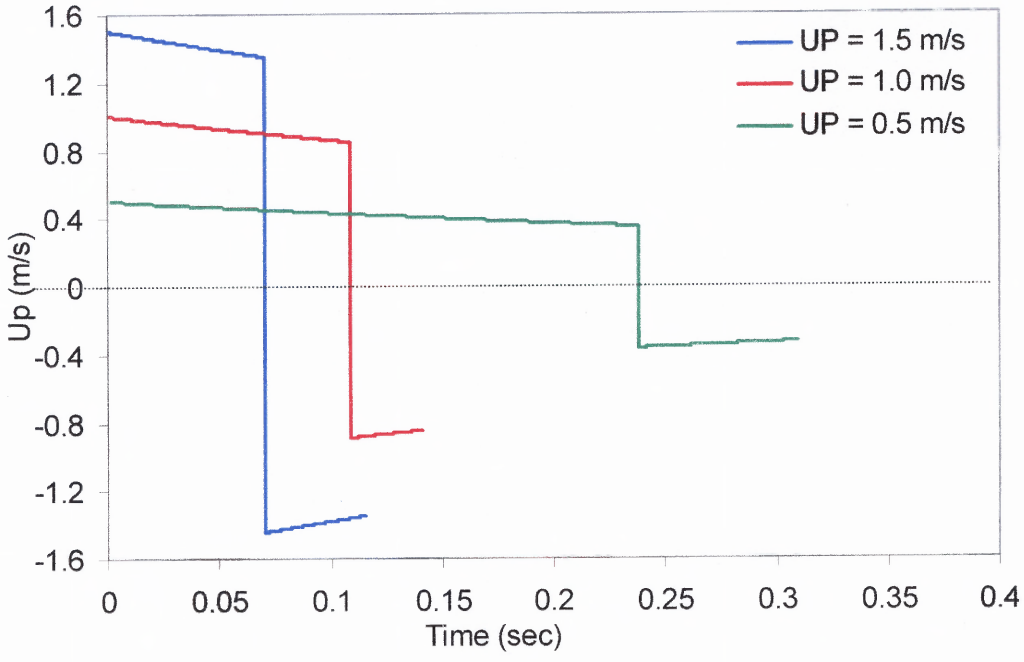

Figure 5.18 Velocity variation of the particle during Leidenfrost collision with different initial velocities.

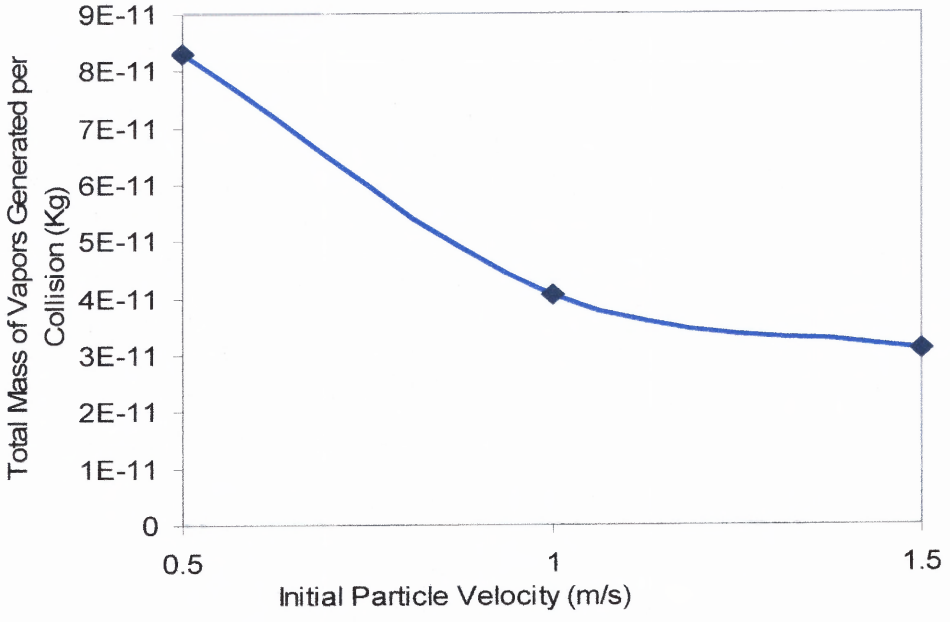

Figure 5.19 Total mass evaporated per collision with different initial velocities.

5.5 Normal Collision Calculations for FCC Particle and Water Surface

The above model is applied to the calculations for parameters during the Leidenfrost collision of FCC particle with water surface. In this case, solid particle density is very low (1480 Kg/m3) as compared to the copper particle (8900 Kg/m3). The particle initial temperature and velocity are 1200 K and 1.5 m/s respectively. This temperature is the same as that of the gas-solid suspension in the riser. However, the effect of porosity of the FCC particle is neglected for simplicity as well as the liquid is simulated with water properties rather than actual oil properties. Another major difference in these calculations is the temperature of the surrounding medium which is at the same temperature as the initial particle temperature i.e., 1200K.

The typical results are shown in the following figures. Figure 5.20 shows the temperature profile of the particle with respect to time. It can be seen clearly from this figure that the particle temperature decreases very slowly during the initial part of the approach. This is due to the reason that the particle is far away from the water surface and its heat loss to the water surface due to conduction and radiation is very small. However, as the particle reaches the water surface, the heat transfer increase rapidly and the temperature of the particle reduces quickly. The temperature of the particle during the rebounding is also reducing at the same rate as during the approach. When the particle moves away from the surface of water the heat transfer reduces the temperature reduction rate also decreases. The temperature change of the particle along its trajectory is shown in the Figure 5.21.

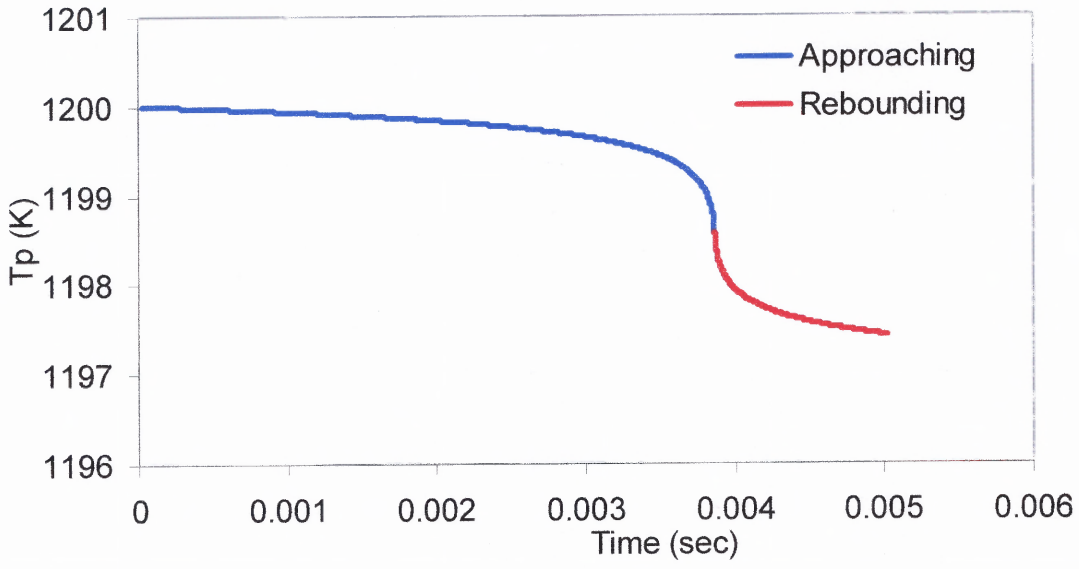

Figure 5.20 Temperature profile of FCC particle during the collision.

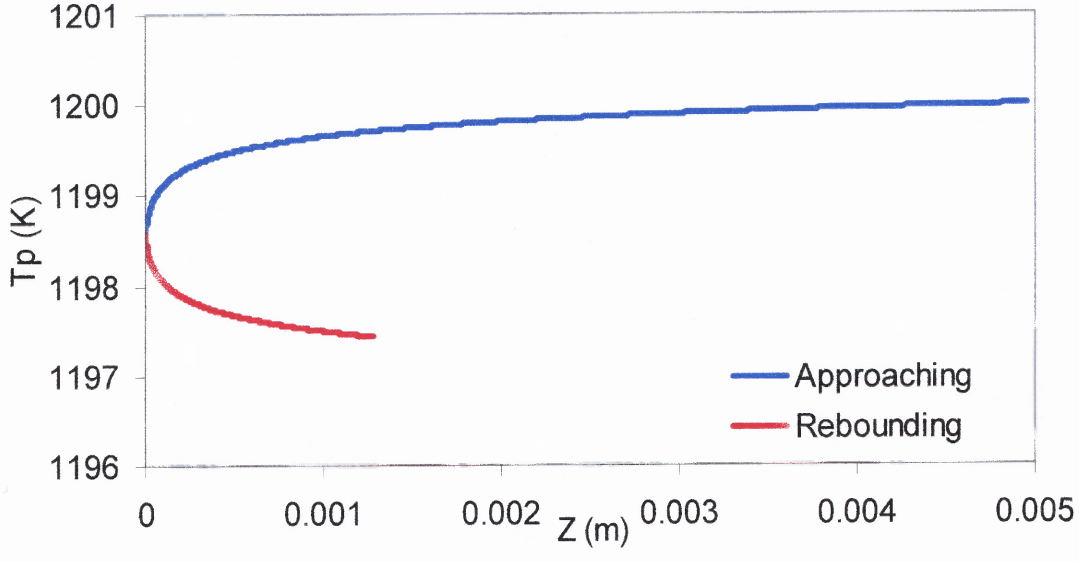

Figure 5.21 Temperature profile of FCC particle along the trajectory.

Figure 5.22 shows the total heat transfer to the liquid during the collision. It can be seen that the maximum heat transfer during the single collision is 0.095 W. This is one order of magnitude less than that of the collision between the copper

particle and water surface. This is due to the reason that the collision time in this case is much less than that of the copper particle case. The limited thermal capacity and size of the FCC particle also restrict the transfer of heat energy during the collision. It is also very interesting to note that the approaching and rebounding heat transfer are precisely symmetric in FCC case.

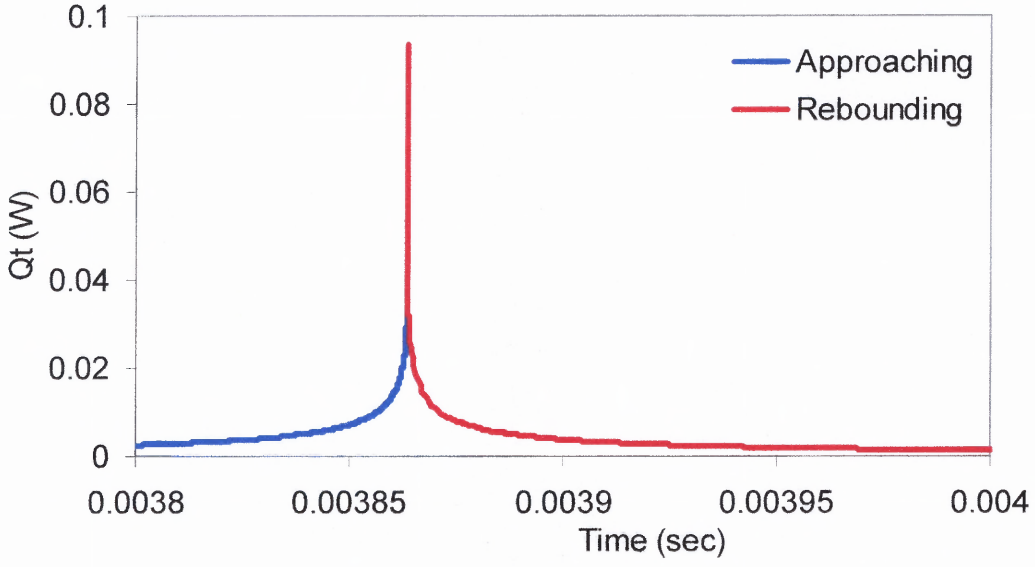

Figure 5.22 Heat transfer to the liquid surface during the collision.

Figure 5.23 shows the velocity profile of the FCC particle during the entire collision process. During the approach the velocity change is very small initially, however, when the particle is very close to water surface and the mass of vapors generated is increased, the net pressure force on the particle is significant. This causes the rapid decrease in the particle velocity, until the particle stops and rebounded under the effect of increasing pressure force. However, as the particle bounces off the

surface, the gap between the particle and water surface increases and hence the particle velocity starts to decrease again.

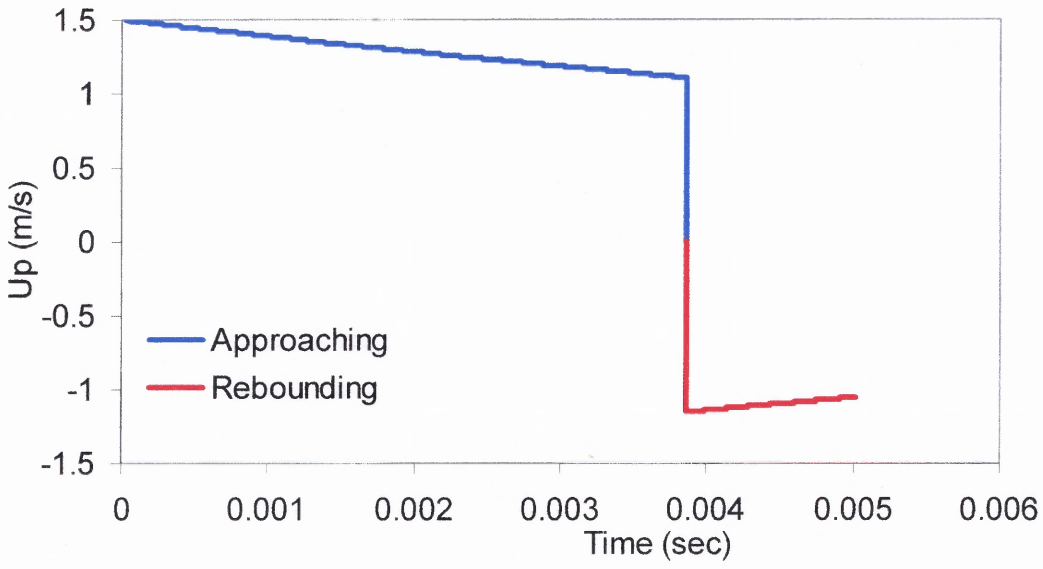

Figure 5.23 Velocity profile of the FCC particle during the collision.

5.6 Tangential Sliding Mechanistic Model of Type II Leidenfrost Collision

A model is developed to calculate the temperature of the water as the solid droplet travels over it. A 2-D model is developed to compute the temperature of the water surface as shown in the figure below,

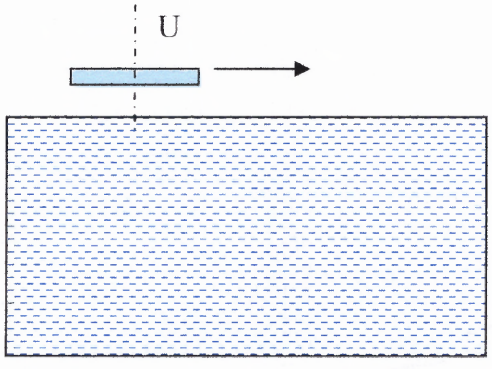

Figure 5.24 Solid disc at very high temperature traveling over the water surface.

The following assumptions are made to simplify the analysis,

- The droplet is a flat disc of radius r
- The temperature of the disc remains constant, Ts
- The temperature of the vapors between the solid and liquid surface is constant, Tvap
- The radiation and convection heat transfer are considered in y-direction only.
- Inner nodes have conduction only.
- Boundaries are insulated.

The nodal diagram and the heat transfer analysis of the model is as shown below,

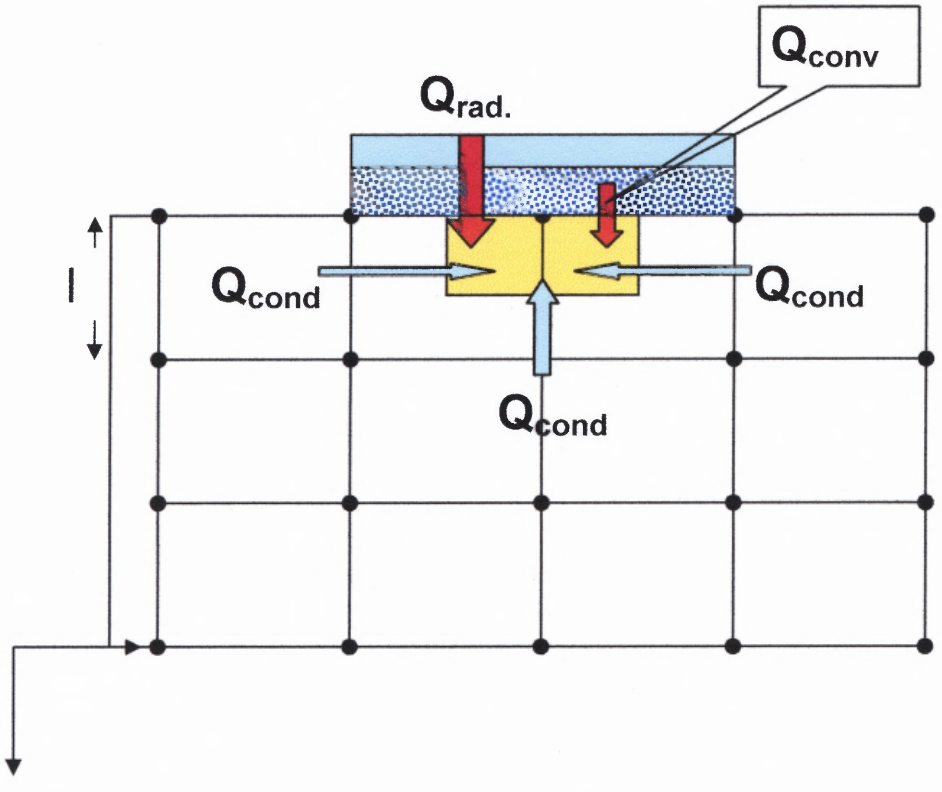

Figure 5.25 Energy balance of the nodal solution for the water temperature.

For any node the energy balance gives the following equation

$$\sum_{AllSide} \dot{Q} + \dot{G}_{element} = \frac{\Delta E}{\Delta t} \tag{5.33}$$

$$\sum_{AllSide} \dot{Q} = \dot{Q}_{cond.LEFT} + \dot{Q}_{cond.RIGHT} + \dot{Q}_{cond.BOTTOM} + \dot{Q}_{conv.TOP} + \dot{Q}_{rad.TOP} \tag{5.34}$$

$$\dot{Q}_{cond.RIGHT} = k \frac{l}{2} \frac{T_{right}^{\ i} - T_{node}^{\ i}}{l} \tag{5.35}$$

$$\dot{Q}_{conv.TOP} = hl(T_{vapor} - T_{node}^{\ i}) \tag{5.36}$$

$$\dot{Q}_{cond.BOTTOM} = kl \frac{T_{bottom}^{\ i} - T_{node}^{\ i}}{l} \tag{5.37}$$

$$\dot{Q}_{cond.LEFT} = k \frac{l}{2} \frac{T_{left}^{\ i} - T_{node}^{\ i}}{l} \tag{5.38}$$

$$\dot{Q}_{rad.TOP} = \varepsilon \sigma l(T^4_{\ surface} - T^4_{\ node}{}^{i}) \tag{5.39}$$

$$\frac{\Delta E}{\Delta t} = \rho V_{element} C \frac{T_{node}^{\ i+1} - T_{node}^{\ i}}{\Delta t} \tag{5.40}$$

where

l=distance between two nodes.

K= thermal conductivity of the water

ρ= density of the water

h= Convective heat transfer coefficient

σ=Stephan Boltzman Constant

ε=emissivity of the solid surface

Δt= time step

By using the above mentioned Equation (5.35) to (5.40) and substituting them in the Equation (5.34), the implicit formulation is written as follows,

$$T_{node}^{i+1} = (1 - 4\tau - 2\tau\frac{hl}{k} - 2\tau\frac{\varepsilon\sigma l}{k}T^3{}_{node}^{\ i})T_{node}^{\ i} + \tau(T^i_{left} + T^i_{right} + 2T^i_{bottom} + 2\frac{hl}{k}T_{vap} + 2\frac{\varepsilon\sigma l}{k}T_s) \quad (5.41)$$

where $\tau = \frac{\alpha\Delta t}{l^2}$ and $\alpha = \frac{k}{\rho C}$

By using the same analogy, appropriate values of element size and the corresponding temperatures, the equations of all the nodes can be written.

5.6.1 Stability Criterion

As $$\tau \leq \frac{1}{(4 - 2\frac{hl}{k} 2\frac{\varepsilon\sigma l}{k}T^3{}_{node}^{\ i})} \quad (5.42)$$

and $$\Delta t \leq \frac{l^2}{\alpha(4 - 2\frac{hl}{k} 2\frac{\varepsilon\sigma l}{k}T^3{}_{node}^{\ i})} \quad (5.43)$$

5.6.2 Important Criterion for Modeling

- The temperature of the node starts increasing once the front edge of disc crosses the node.
- Once the back edge of the disc leaves the node, the node starts loosing the heat to the environment.
- If the temperature of a node is reached to 100, the temperature remains the constant and the additional heat supplied to the node is consumed in the phase change of the water (not included in calculations of this project).

5.6.3 Initial and Boundary Conditions

At t=0, all temperatures are room temperature.

The boundaries are insulated, so no heat transfer occurs across the boundaries.

5.6.4 Case Study

U =0.02 m/s, T_s =1100 C

T_∞ =20 C, T_{vap}=500 C,

h_{air}=100 W/m^2-C k =0.654 W/m-C

ρ =983 Kg/m^3 C =4185 J/Kg-C

ε =0.19

using a 5*3 nodes

Mesh length = 0.000704 m

Δt=0.000352 sec and Velocity of the disc is 0.04 m/s

Using all these values in the model developed, the temperature of any node can be found for the entire time range.

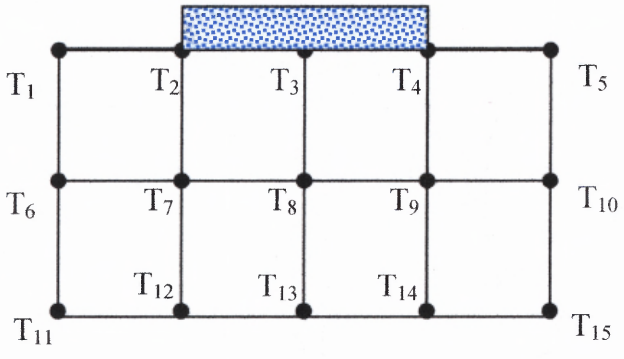

Figure 5.26 A 5 x 3 mesh for the current case study.

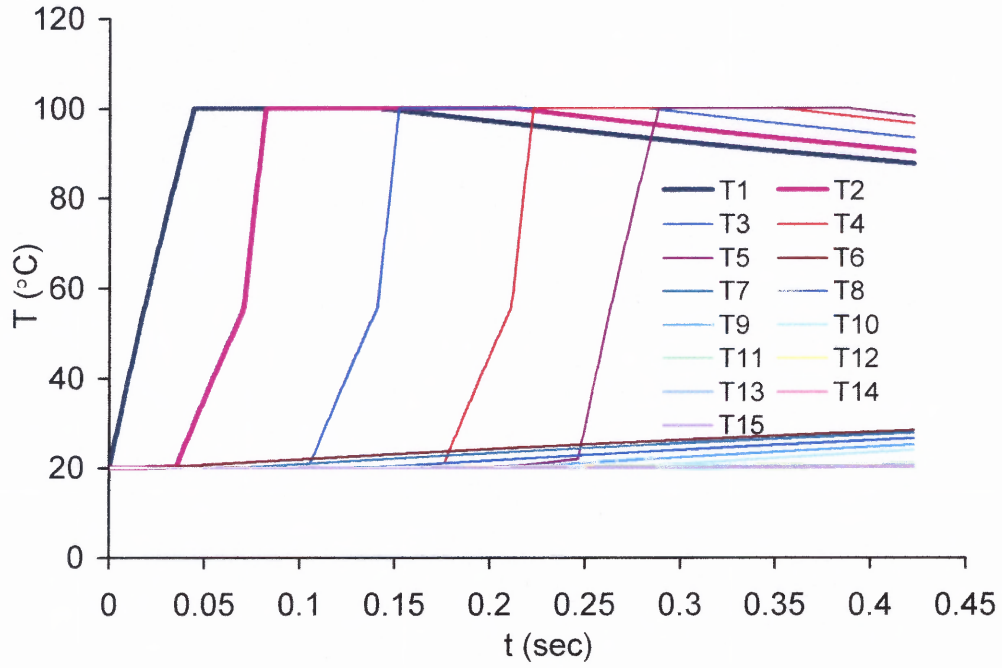

Figure 5.27 Temperature profiles for all nodes.

The temperature plot of all the nodes is shown in the Figure 5.23. The temperature T_1 of the very first node (Top left boundary node) is increasing as the disc is moving over it. The radiation heat transfer from the disc causes the temperature to increase and reach 100 C at 0.044 sec. After that the temperature of the node stays constant at 100 C and the phase change from liquid water to water vapor starts. As soon as the disc leaves the node T1 (at 0.1408 sec), the temperature of the node starts decreasing as the heat is now being released from the water to the atmosphere due to convection. For Node 2 which is the top inner node, as soon as the edge of the disc comes in contact with the node element. There are two different slopes of the line, which is due to the assumption that only the half of the node is under the influence of the radiation from disc and convection through vapor layer for

the time until the front edge of the disc reaches the node. After that the entire node element is under the influence of the radiation and convection. The node starts to loose the energy as soon as the trailing edge of the disc leaves the node as mentioned above.

The only heat transfer to the second layer from top is the conduction through the neighboring nodes, so the increase in the temperature is almost linear. Even though the disc is not at the top layer node, but still the top node is at a higher temperature than the lower nodes, so the heat transfer from top layer to bottom layer continues.

5.7 Conclusions

Experimental study is conducted to identify the different modes of type II Leidenfrost collision. A mechanistic model is developed to simulate the normal collision of the solid particle with large droplet. This model is based on the heat and mass transfer between the liquid and solid surface. Heat due to conduction and radiation are taken into effect. A 2-D model is developed to study the reverse Leidenfrost collision between the hot solid particle and the water surface. The energy balance at every node provides the temperature history of that node. Although, the mesh size is very precise and the adjustable parameter h_{conv} need to be verified, the model predicts the temperature profiles with reasonable qualitative agreement.

5.8 Future Work

Despite the fact that this topic of spray structure is very complicated, there still remain so many unanswered questions. So in future there may be many challenging research areas regarding this topic. Although very primitive heat transfer models were developed in this study, however, these models need to be improved. A more sophisticated model should consider the curvature effect of the solids, size ratio, and limited heat capacity of the solids as well as the oblique collision mechanism.

CHAPTER 6

CONCLUSIONS

This study is conducted into three parts. Albeit, these three parts are studied discretely, it is important to note that there is a strong connection among the three parts. In the first part, entrainments capabilities of two phase jets are explored with respect to the similarity criterion, entrainment velocities, entrainment momentum ratio and evaporation rate along the jet trajectory. Similarity co-relations are recognized which have laid down the foundation for the development of mechanistic model. The distribution of evaporation rate along the jet trajectory is experimentally calculated which is a deterministic factor for spray flow characteristics. This study shows that the vaporization of spray weakens the jet entrainment. In the second part, quantitative and qualitative results of flow characteristics are obtained for various sprays with rectangular nozzle configuration and fan angles. Three-dimensional numerical study results yield complete flow information such as, spray penetration, spray deflection, solids concentration, gas temperature profiles as well as evaporation rate along the jet trajectory. It shows that the higher the fan angle, the higher total mass evaporated rate is. This study demonstrates that the flow characteristics can be controlled effectively by the combination of nozzle configuration and fan angle. After understanding the flow characteristics, it is concluded that the flow characteristics mainly depend on the phase transport during the solid and liquid collision. This phase transport is based on the heat and mass transfer during the collision of a small solid particle with a large droplet. This is defined as Type II Leidenfrost collision. So the

focus is on the interaction mechanism between the small solid particle and large liquid surface. Experimental investigations established three different modes of collision dynamics with uniquely associated heat transfer to each mode. Basic mechanistic model is developed for the normal collision which incorporates all the fundamental important physics of the contact mechanism. A parametric study on some governing parameters such as the initial temperature of the particle or initial velocity of the particle is performed. It is also shown that the model is applicable to the FCC particle (with no porosity) as well. This model lays the pioneering work to answer the challenging questions regarding the interaction mechanisms of three phase flow structures which in turn governs the flow characteristic of spray jet inside gas-solid suspensions.

REFERENCES

1. Abramovich G. N., (1963). The theory of turbulent jets, M I. T. Press, MA (English translation).

2. Davoust, L. A., Hammoumi, J.L., El, M., (2002). Air entrainment by a plunging jet: the dynamical roughness concept and its estimation by a light absorption technique, International Journal of Multiphase Flow, 28, 1541-1564.

3. Fincke, J.R., Crawford, D.M., Snyder, S.C., Swank, W.D., Haggard, D.C., Williamson, R.L., (2003). Entrainment in high-velocity, high-temperature plasma jets. Part I: experimental results, International Journal of Heat and Mass Transfer, 46, 4201-4213.

4. Williamson, R.L., Fincke, J.R., Crawford, D.M., Snyder,S.C., Swank,W.D., Haggard, D.C., (2003). Entrainment in high-velocity, high-temperature plasma jets. Part II: computational results and comparison to experiment, International Journal of Heat and Mass Transfer, 46, 4215-4228.

5. Park, T.W., Katta, V.R., Aggarwal, S.K., (1998). On the dynamics of a two-phase non-evaporating swirling jet, International Journal of Multiphase Flow, 24, 295-317.

6. Ghosh, S., Hunt, J.C., (1998). Spray jets in a cross-flow, Journal of Fluid Mechanics, 365, 109-136.

7. Han, D., Mungal, M.G., (2001). Direct measurement of entrainment in reacting/nonreacting turbulent jets, Combustion and Flame, 124, 370-386.

8. Yang, W. C., Keairns, D.L., (1982). Solid entrainment rate into gas and gas-solid two phase jets in a fluidized bed, Powder Technology, 33, 89-94.

9. Filla, M., Massimilla, L., Vaccaro, S., (1983). Gas jets in fluidized beds: the influence of particle size, shape and density on gas and solid entrainment, Int. Journal of Multiphase Flow, 9, 259-267.

10. Park, S.H., and Shin, H.D., (1993). Measurement of entrainment characteristics of swirling jets, International Journal of Heat and Mass Transfer, 36, 4009-4018.

11. Wang, X., Zhu, C., Ahluwalia, R., (2004). Numerical simulation of evaporating spray jets in concurrent gas-solid pipe flows, Powder Technology, 140, 56-67.

12. Wang, X., (2002). Concurrent evaporating spray jet in dilute gas-solid pipe flows, Ph.D. Thesis, New Jersey Institute of Technology, NJ.

13. Wang, X., Zhu, C., (2003). Concentric evaporating spray jets in dilute gas-solids pipe flows, Powder Technology, 129, 59–71.

14. Rajaratnam, N., (1973). Developments in Water Science, Elsevier.

15. Sirignano, W.A., (1999). Fluid Dynamics and Transport of Droplets and Sprays, Cambridge University Press.

16. Kouremenos, D., Pantzas, C., Panagakls, G., Krikkls, R., (1995). Thermodynamics and the Design, Analysis, and Improvement of Energy Systems, 35, 261-273,

17. Skouby, D.C., (1998). Hydrodynamics Studies in a 0.45-m riser with Liquid Feed Injection, Proceeding of AIChE Annual Meeting, 238.

18. Fan, L. -S., Lau, R., Zhu, C., Vuong, K., Warsito, W., Wang, X., Liu, G., (2001). Evaporative liquid jets in gas-liquid–solid flow system, Chemical Engineering Science, 56, 5871-5891.

19. Zhu, C., Wang, X., Fan, L.-S., (2000). Effect of solid concentration on evaporative liquid jets in gas-solid flows, Powder Technology, 111, 79-82.

20. Zhu, C., Liu, G., Wang, X., and Fan, L.-S., (2002). A parametric model for evaporating liquid jets in dilute gas-solid flows, International Journal of Multiphase Flow, 28, 1479-1495.

21. Mirgain, C., Briens, C., Pozo, M. D., Loutaty, R., Bergougnou, M, (2000). Modeling of feed vaporization in fluid catalytic cracking, Industrial Engineering Chemical Research, 39, 4392-4399.

22. Gao, J., Zu, C., Lin, S., Yang, G., (2001). Simulations of gas-liquid –solid 3-phase flow and reaction in FCC riser reactors. AIChE Journal, 47, 152-156.

23. Chang, S.L., Lottes, S.A., Zhou C.Q., Petrick, M., (1996). Evaluation of multi-phase heat transfer and droplet evaporation in petroleum cracking flows, Proceeding of ASME Heat Transfer Division, 4, 17-27.

24. Zhu, C., Wang, X., Liu, G., (2002). Effect of particle loading on liquid nitrogen jet mixing in a FCC riser, Circulating Fluidized Bed Technology, VII, 881-888.

25. Zhu, C., Liu, G., Wang, X., (2002). Oblique evaporating sprays in gas-solid suspensions, ASME Fluid Engineering Division Summer Meeting, 156-161.

26. Pedersen, C.O., (1970). An experimental study of the behavior and heat transfer characteristics of a water droplet impinging upon a heated surface, International Journal of Heat Mass Transfer, 13, 369-381.

27. Wachters, L.H.J., and Westerling, N.A.J., (1966). The heat transfer from a hot wall to impinging water drops in the spheroidal state, Chemical Engineering Science, 21, 1047-1056.

28. Akao, E., Araki, K., Mori, S., Moriyama, A., (1980). Deformation behaviors of a liquid droplet impinging onto hot metal surface, Trans. Int. Steel Inst. Japan (ISIJ), 20, 737-743.

29. Ueda, T., Enomota, T., Kanetsuki, M., (1979). Heat transfer characteristics and dynamic behavior of saturated droplets impinging on a heated vertical surface, Bulletin of the JSME, 22, 724 -732.

30. Hatta, N., Fujimoto H. and Takuda, H., (1995). Deformation process of a water droplet impinging on a solid surface, Translation of the ASME Journal of Fluids Engineering, 117, 394-401.

31. Hatta, N., Fujimoto, H., Kinoshita, K., Takuda, H., (1997). Experimental study of deformation mechanism of a water droplet impinging on hot metallic surfaces above the Leidenfrost temperature, Translation of the ASME Journal of Fluids Engineering, 119, 692-699.

32. Bernardin, J.D., Stebbins, C.J., Mudawar, I., (1997). Mapping of impact and heat transfer regimes of water drops impinging on a polished surface, International Journal of Heat Mass Transfer, 40, 247-267.

33. Karl, A., and Frohn, A., (2000). Experimental investigation of interaction processes between droplets and hot walls, Physics of Fluids, 12, 785-796.

34. Bolle, L., and Moureau, J.C., (1976). Spray cooling of hot surfaces. Multiphase Science and Technology, 1092.

35. Makino, K., and Michiyoshi, I., (1984). The behavior of a water droplet on heated surfaces, International Journal of Heat Mass Transfer, 27, 781-791.

36. Buyevich, Y. A., and Mankevich, V.N., (1995). Interaction of a dilute mist flow with a hot body, International Journal of Heat Mass Transfer, 38, 731-744.

37. Chaar, S., (2002). Experimental study of Leidenfrost collision between particles and droplets. Master's Project Report, New Jersey Institute of Technology.